



Source details

Annals of Nuclear Energy

Formerly known as: Annals of Nuclear Science and Engineering

Scopus coverage years: from 1975 to Present

Publisher: Elsevier

ISSN: 0306-4549 E-ISSN: 1873-2100

Subject area: Energy: Nuclear Energy and Engineering

Source type: Journal

CiteScore 2022

3.6



SJR 2022

0.859



SNIP 2022

1.253



[View all documents >](#)

[Set document alert](#)

[Save to source list](#) [Source Homepage](#)

[CiteScore](#) [CiteScore rank & trend](#) [Scopus content coverage](#)

i Improved CiteScore methodology



CiteScore 2022 counts the citations received in 2019-2022 to articles, reviews, conference papers, book chapters and data papers published in 2019-2022, and divides this by the number of publications published in 2019-2022. [Learn more >](#)

CiteScore 2022 ▼

$$3.6 = \frac{9,682 \text{ Citations 2019 - 2022}}{2,665 \text{ Documents 2019 - 2022}}$$

Calculated on 05 May, 2023

CiteScoreTracker 2023 ⓘ

$$3.6 = \frac{9,291 \text{ Citations to date}}{2,579 \text{ Documents to date}}$$

Last updated on 05 August, 2023 • Updated monthly

CiteScore rank 2022 ⓘ

Category	Rank	Percentile
Energy		
└ Nuclear Energy and Engineering	#24/68	65th

[View CiteScore methodology >](#) [CiteScore FAQ >](#) [Add CiteScore to your site](#)

About Scopus

[What is Scopus](#)

[Content coverage](#)

[Scopus blog](#)

[Scopus API](#)

[Privacy matters](#)

Language

[日本語版を表示する](#)

[查看简体中文版本](#)

[查看繁體中文版本](#)

[Просмотр версии на русском языке](#)

Customer Service

[Help](#)

[Tutorials](#)

[Contact us](#)

ELSEVIER

[Terms and conditions ↗](#) [Privacy policy ↗](#)

Copyright © Elsevier B.V. ↗. All rights reserved. Scopus® is a registered trademark of Elsevier B.V.

We use cookies to help provide and enhance our service and tailor content. By continuing, you agree to the use of cookies ↗.



Annals of Nuclear Energy

COUNTRY

United Kingdom

Universities and research
institutions in United KingdomMedia Ranking in United
Kingdom**SUBJECT AREA AND CATEGORY**Energy
└ Nuclear Energy and
Engineering**PUBLISHER**

Elsevier Ltd.

H-INDEX

77

PUBLICATION TYPE

Journals

ISSN

03064549, 18732100

COVERAGE

1975-2023

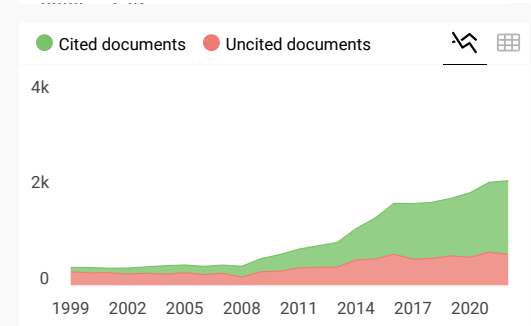
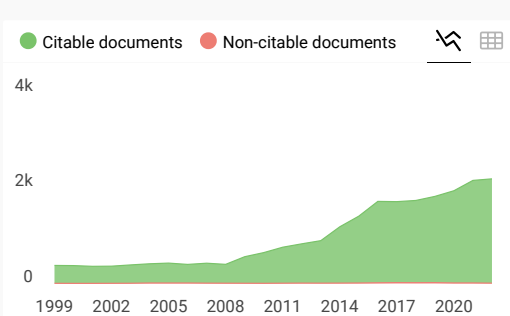
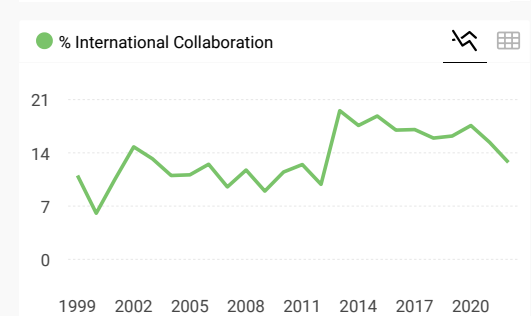
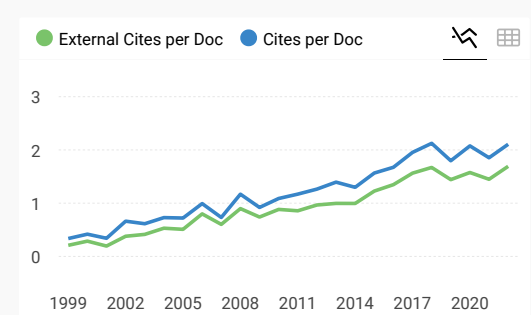
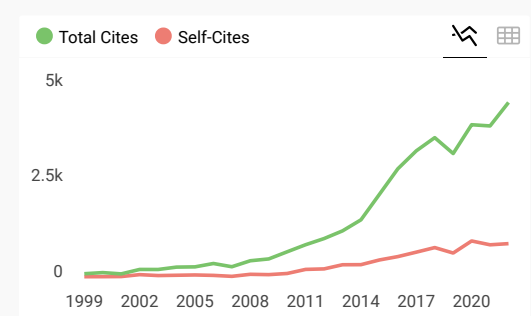
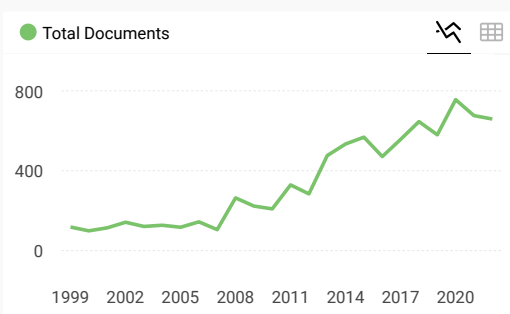
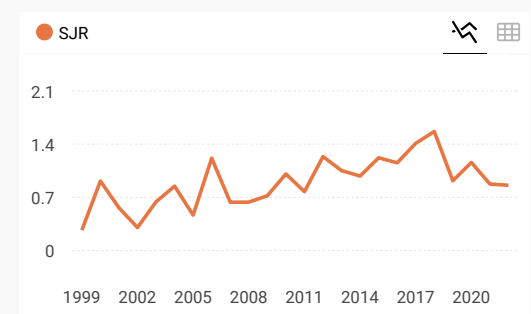
INFORMATION[Homepage](#)[How to publish in this journal](#)[Contact](#)**SCOPE**

Annals of Nuclear Energy provides an international medium for the communication of original research, ideas and developments in all areas of the field of nuclear energy science and technology. Its scope embraces nuclear fuel reserves, fuel cycles and cost, materials, processing, system and component technology (fission only), design and optimization, direct conversion of nuclear energy sources, environmental control, reactor physics, heat transfer and fluid dynamics, structural analysis, fuel management, future developments, nuclear fuel and safety, nuclear aerosol, neutron physics, computer technology (both software and hardware), risk assessment, radioactive waste disposal and reactor thermal hydraulics. Papers submitted to Annals need to demonstrate a clear link to nuclear power generation/nuclear engineering. Papers which deal with pure nuclear physics, pure health physics, imaging, or attenuation and shielding properties of concretes and various geological materials are not within the scope of the journal. Also, papers that deal with policy or economics are not within the scope of the journal.



Join the conversation about this journal

<p>1 Progress in Nuclear Energy</p> <p>GBR</p> <p>82% similarity</p>	<p>2 Kerntechnik</p> <p>DEU</p> <p>81% similarity</p>	<p>3 Hedongli Gongcheng/Nuclear Power Engineering</p> <p>CHN</p> <p>76% similarity</p>	<p>4 Science and Technology of Nuclear Installations</p> <p>EGY</p> <p>76% similarity</p>	<p>5 Nuclear Engineering and Technology</p> <p>USA</p>
--	---	--	---	---



Annals of Nuclear Energy ← Show this widget in your own website

Q1 Nuclear Energy and Engineering
best quartile

SJR 2022
0.86

powered by scimagojr.com

Just copy the code below and paste within your html code:

```
<a href="https://www.scimaç
```



annals of NUCLEAR ENERGY

Executive Editors

L. Cao
Xi'an Jiaotong University, Xi'an, China

E. Gilad
Ben-Gurion University of the Negev, Be'er Sheva, Israel

S. Pozzi
University of Michigan, Ann Arbor, Michigan, USA

P. Ravetto
Politecnico di Torino, Torino, Italy

EXECUTIVE EDITORS

L. CAO
*Xi'an Jiaotong University,
Xi'an, China*

E. Gilad
*Ben-Gurion University of the
Negev, Be'er Sheva, Israel*

S. POZZI
*University of Michigan,
Ann Arbor, Michigan, USA*

P. RAVETTO
*Polytechnic of Turin,
Torino, Italy*

EXECUTIVE EDITOR EMERITUS

M. GHIAASIAAN
Georgia Institute of Technology, Atlanta, Georgia, USA

ASSOCIATE EDITORS

I. BOLOTNOV
*NC State University,
Department of Nuclear Engineering,
Raleigh, North Carolina, USA*

M. HURSIN
*Paul Scherrer Institute,
Villigen, Switzerland*

Y. YANG
*Shanghai Jiao Tong University School
of Mechanical Engineering,
Shanghai, China*

HONORARY EDITOR

I. PÁZSIT
Chalmers University of Technology, Gothenburg, Sweden

ADVISORY EDITORS

G. CHIBA
Hokkaido University, Sapporo, Japan

N.Z. CHO
*Korea Advanced Institute of Science and Technology,
Daejeon, South Korea*

S. DULLA
Polytechnic of Turin, Torino, Italy

J. FAVORITE
*Los Alamos National Laboratory, Los Alamos, New Mexico,
USA*

N. GARCIA-HERRANZ
*Polytechnic University of Madrid Superior Technical School of
Mines and Energy, Madrid, Spain*

H.G. JOO
Seoul National University, Seoul, South Korea

D. KASTANYA
Kinectrics, Toronto, Ontario, Canada

D. LEE
*Ulsan National Institute of Science and Technology,
Ulsan, South Korea*

J.I. LEE
*Korea Advanced Institute of Science and Technology,
Daejeon, South Korea*

J. LEPPÄNEN
*VTT Technical Research Centre of Finland Ltd, VTT,
Finland*

Y. LI
*Xi'an Jiaotong University School of Energy and Power
Engineering, Department of Nuclear Science and Technology,
Xian, China*

S. LOYALKA
University of Missouri, Columbia, Missouri, USA

F. NIU
*North China Electric Power University, School of Nuclear
Science and Engineering, Beijing, China*

C. PAN
*City University of Hong Kong, Department of Mechanical
Engineering, Hong Kong, China*

G.T. PARKS
University of Cambridge, Cambridge, UK

A. PRINJA
*The University of New Mexico, Albuquerque, New Mexico,
USA*

C.H. PYEON
*Kyoto University Research Reactor Institute, Sennan-gun,
Japan*

F. RAHNEMA
Georgia Institute of Technology, Atlanta, Georgia, USA

R. SANCHEZ
*French Alternative Energies and Atomic Energy Commission
Systems and Structures Modelling Department,
Gif-sur Yvette, France*

P.H. SEONG
*Korea Advanced Institute of Science and Technology,
Daejeon, South Korea*

W. TIAN
Xi'an Jiaotong University, Xi'an, China

M. UEMATSU
*Nuclear Damage Compensation and Decommissioning
Facilitation Corporation, Minato-Ku, Japan*

K. VELUSAMY
Indira Gandhi Centre for Atomic Research, Kalpakkam, India

K. VIEROW
*Texas A&M University, College Station, College Station, Texas,
USA*

J. WANG
*University of Wisconsin-Madison, Department of Engineering
Physics, Madison, Wisconsin, USA*

Z. WU
*Virginia Commonwealth University, Department of Mechanical
and Nuclear Engineering, Richmond, Virginia, USA*

J. XIONG
*Shanghai Jiao Tong University School of Mechanical
Engineering, Shanghai, China*

T. YAMAMOTO
Kyoto University, Kyoto, Japan

D. ZHANG
*Xi'an Jiaotong University School of Energy and Power
Engineering, Department of Nuclear Science and Technology,
Xian, China*

J. ZHAO
City University of Hong Kong, Hong Kong, Hong Kong

W. ZWERMANN
*Gesellschaft für Anlagen- und Reaktorsicherheit GmbH
Garching, Garching bei München, Germany*

Volume 172

July 2022

[Download full issue](#)

[← Previous vol/issue](#)

[Next vol/issue >](#)

Receive an update when the latest issues in this journal are published

[Sign in to set up alerts](#)

Full text access

Editorial Board

Article 109135

[View PDF](#)

Review Article

Review article *Open access*

In-situ testing of Czech bentonite for radioactive waste disposal in Mock-up Josef experiment

J. Štáštka, I. Hanusová, L. Hausmannová, M. Kučerová

Article 109059

[View PDF](#) [Article preview](#) [v](#)

Research Articles

Research article Abstract only

Optimal design of separation cascades using the whale optimization algorithm



Remon Ibrahim, Adriaan Buijs, John Luxat

Article 109056

Article preview

Research article Abstract only

Fluid-structure coupled vibration characteristics of liquid immersed square channels within confinement

Gaurav Verma, M. Eswaran, Shaji Mammen, S.D. Sajish

Article 109061

Article preview

Research article Abstract only

A comprehensive Bayesian framework for the development, validation and uncertainty quantification of thermal-hydraulic models

Riccardo Cocci, Guillaume Damblin, Alberto Ghione, Lucia Sargentini, Didier Lucor

Article 109029

Article preview

Research article Abstract only

On integrating Monte Carlo calculations in and around near-critical configurations – I. Methodology

M. Brovchenko, K.W. Burn, P. Console Camprini

Article 109063

Article preview

Research article Abstract only

Inherent safety enhancement by design optimization of a floating absorber for safety at transient (FAST) in an advanced burner reactor

Seongmin Lee, Yong Hoon Jeong

Article 109026

Article preview

Research article Abstract only

Mitigation of long-term station blackout accident of advanced boiling water reactors

Min Lee, Yu Min Chen, Yu Sheng Wang

Article 109074

Article preview

Research article Abstract only



Research article Abstract only

Research on the energy characteristics of reactor coolant pump under flow coastdown transient

Ye Daoxing, Liu Anlin, Luo Yimin, Chen Junlin, ... Gou Qiuqin

Article 109081

Article preview

Research article Abstract only

Effect of thermo-physical properties of accident tolerant fuels on transient fuel behaviors and the safety

Sihong He, Jiejun Cai, Honghao Yu, Xuezhong Li, Rong Liu

Article 109080

Article preview

Research article Abstract only

A medium temperature heat pipe cooled reactor

S.N. Li, Z.T. Liang, B.H. Yan

Article 109068

Article preview

Research article Abstract only

Statistical characterization of liquid film fluctuations during gas-liquid two-phase counter-current flow in a 1/30 scaled-down test facility of a pressurized water reactor (PWR) hot leg

Achilleus Hermawan Astyanto, Josi Aldo Emmanuel Pramono, I.G.N.B. Catrawedarma, Deendarlianto, Indarto

Article 109065

Article preview

Research article *Open access*

REGAL International Program: Analysis of experimental data for depletion code validation

J. Eysermans, M. Verwerft, K. Govers, R. Ichou, ... N. Slosse

Article 109057

 [View PDF](#) Article preview

Research article Abstract only

Evaluation of service reliability of AP1000 nuclear reactor coolant pump rotor-can

Yan Cui, Chi Zhang, Liwen Zhang, Kangjie Song

Article 109073

Article preview

Research article Abstract only



Research article ● [Open access](#)

A new methodology for thermal analysis of geological disposal of spent nuclear fuel using integrated simulations of gamma heating and finite element modeling

Peter Jansson, Peter Renström, Jan Sarnet, Anders Sjöland
Article 109082

 [View PDF](#) [Article preview](#) ✓

Research article Abstract only

Particulate Fuel Modeling of MC²-3 using Iterative Local Spatial Self-shielding Method

H. Park, W.S. Yang, C.H. Lee
Article 109060

[Article preview](#) ✓

Research article Abstract only

Exponential fitting of PWR decay heat data at short cooling time for use in the PRESTO experiment

Francesco Muratori, Frédéric Nguyen, Christophe Le Niliot, Christian Gonnier, Romain Eschbach
Article 109064

[Article preview](#) ✓

Research article Abstract only

Development of 3-D numerical methodology to investigate transient characteristics of fuel temperature and hydrated residual water during drying process of dry storage system

Y.S. Tseng, W.Y. Wang, C.H. Lin, Y.M. Ferng, M.H. Wan
Article 109083

[Article preview](#) ✓

Research article Abstract only

Numerical simulation of sodium mist behavior in turbulent Rayleigh-Bénard convection using new developed mist models

Hiroaki Ohira, Masaaki Tanaka, Ryuji Yoshikawa, Toshiki Ezure
Article 109075

[Article preview](#) ✓

Research article Abstract only

A multiphysics model of the versatile test reactor based on the MOOSE framework

Nicolas Martin, Ryan Stewart, Sam Bays
Article 109066

[Article preview](#) ✓



Research article Abstract only

Experimental study on combustion characteristics of mixed sodium fire in a well-ventilated environment compared with confined space

Yao-long Ma, Zhi-gang Zhang, Hai-su Du, Ke-liang Li, ... Xin-wen Wang

Article 109069

Article preview

Research article Abstract only

Experimental study and analysis on the interfacial drag of two-phase flow in porous media

Haoxiang Zhao, Liangxing Li, Xiangyu Li, Zhengzheng Zhang

Article 109085

Article preview

Research article Abstract only

Research on proportional method for experimental facility of lead-based fast reactor with natural circulation

Pengcheng Zhao, Ting Wang, Enping Zhu, Tianshi Wang, Yuxuan Wang

Article 109096

Article preview

Research article Abstract only

Experimental study of heat distribution in a Non-uniform heat source of a natural circulation loop

Solomon Bello, Puzhen Gao, Samuel Abiodun Olatubosun, Yuqi Lin, John Njoroge

Article 109076

Article preview

Research article Abstract only

Numerical study on pressure oscillations amplitude distribution induced by water flow into pipe filled with steam

Abdul Quddus, Ajmal Shah, Kamran Rasheed Qureshi, Ahmad Tahir, ... Muhammad Khawar Ayub

Article 109095

Article preview

Research article Abstract only

Development and verification of Geant4-based parallel computing Monte Carlo simulations for nuclear logging applications

Yang Wang, Jingang Liang, Qiong Zhang, Xinyang Wang, ... Ye Chen

Article 109079

Article preview



Article preview ▾

Research article Abstract only

An optimized numerical method on corrosion in the non-isothermal lead–bismuth eutectic loops with solid–phase oxygen control system

Xiaobo Li, Ruixian Liang, Yifeng Wang, Huiping Zhu, ... Fenglei Niu
Article 109084

Article preview ▾

Short Communication

Short communication Abstract only

Experimental analysis of droplet impacting on inclined wall of the corrugated plate dryer in steam generator of nuclear power plants

Li Ru, Chen Bowen, Wang Weibing, Wang Bo, Tian Ruifeng
Article 109062

Article preview ▾

Short communication Abstract only

Reactor physics study of square and hexagonal lattice cell using MANTRA (Method of ChAracteristics based Neutron TRAnsport Code) coupled with resonance treated multi energy group cross section library

Tanay Mazumdar, Tej Singh
Article 109072

Article preview ▾

[← Previous vol/issue](#)

[Next vol/issue >](#)

ISSN: 0306-4549

Copyright © 2023 Elsevier Ltd. All rights reserved





Statistical characterization of liquid film fluctuations during gas-liquid two-phase counter-current flow in a 1/30 scaled-down test facility of a pressurized water reactor (PWR) hot leg



Achilleus Hermawan Astyanto^{a,c}, Josi Aldo Emmanuel Pramono^a, I.G.N.B. Catrawedarma^d, Deendarlianto^{a,b}, Indarto^{a,b,*}

^a Department of Mechanical and Industrial Engineering, Universitas Gadjah Mada, Jl. Grafika No. 2, Kampus UGM, Yogyakarta 55281, Indonesia

^b Center of Energy Studies, Universitas Gadjah Mada, Sekip K-1A Kampus UGM, Yogyakarta 55281, Indonesia

^c Department of Mechanical Engineering, Universitas Sanata Dharma, Kampus III USD Maguwoharjo, Yogyakarta 55282, Indonesia

^d Department of Mechanical Engineering, Politeknik Negeri Banyuwangi, Jalan Raya Jember km. 13, Lebanasem, Banyuwangi 68461, Indonesia

ARTICLE INFO

Article history:

Received 7 October 2021

Received in revised form 30 December 2021

Accepted 8 March 2022

Keywords:

Counter-current flow

Hot leg PWR

Parallel-wire probe

Wavelet analysis

ABSTRACT

The present work investigates the statistical characteristics of the fluctuations of the liquid film thickness obtained by resistive-conductance probe signals of a complex geometry representing a 1/30 down-scaled of a PWR hot leg. Here, four locations at the horizontal part of the test section were assessed, while the flow development was investigated through a close observation by using a high-speed video camera. Next, the normalized voltages, indicating the liquid film thickness fluctuations, are shown in the time-series. From the fluctuations, the amplitudes representing the film thickness were recorded. Hence, such statistical diagnostic tools were applied on the basis of time-domain, frequency-domain and also time-frequency domain analyses. From the probability density function, the distributions of the fluctuations were assessed, whereas the power spectral density function describes the dominant frequencies. In addition, the Kolmogorov entropy denotes the chaotic level of the signal, meanwhile the wavelet energy corresponds to several details on the wavy interfaces on the basis of its frequency scales. Next, those parameters were statistically employed to elaborate the interfacial behaviors due to the signal characteristics. The results indicate that the low dominant frequency corresponds to the occurrence of either liquid blockage or slugs during the acquisition, meanwhile the largest scale fluctuations reveal the wave movements.

© 2022 Published by Elsevier Ltd.

1. Introduction

During a loss of coolant accident scenario which can hypothetically occur in the primary circuit of a pressurized water reactor (PWR), the condensate flows along the hot leg counter-currently with the steam. Under the condition of low gas flow rates, a stable counter-current flow occurs. This flow condition is stable for certain both liquid and gas flow rates, in which the gas flows counter-currently with the liquid in a smooth interface (Deendarlianto et al., 2012). The gradual increase of gas flow causes progressively dynamic effects of the liquid flow leaving the hot leg into the reactor pressure vessel (RPV). As time progress, it initiates a limitation at a certain point in which the gas velocity

reaches a maximum value to keep the counter-current flow between the steam and condensate. It is well known as the onset of flooding or counter-current flow limitation (CCFL). A further increase of the gas velocity triggers the liquid to partially flow co-currently with the gas along the hot leg. At a certain next moment, there will be a point in which the liquid will not flow into the reactor core by the increase of the gas flow because it is totally entrained by the gas co-currently. This is called as zero liquid penetration (ZLP). The region between the onset of flooding and the ZLP is known as the partial delivery region (PDR) or flooding regime. During the PDR, the condensate flows partially co-current with the steam. When the water level in the reactor core decreases further, the steam generator dries out in its U-tube, and the natural circulation of the liquid is finished. Here, the amount of heats that can be removed by the two-phase flow strongly depends on the flow regimes in the hot leg (Petritsch & Mewes, 1999).

* Corresponding author at: Department of Mechanical and Industrial Engineering, Universitas Gadjah Mada, Jl. Grafika No. 2, Kampus UGM, Yogyakarta 55281, Indonesia.

E-mail address: indarto@ugm.ac.id (Indarto).

Nomenclature

Symbols

J_G	Gas superficial velocity (m/s)
J_L	Liquid superficial velocity (m/s)
l/D	Riser length to diameter ratio (-)
x/L_H	Probe location/locus (-)
V/V_{max}	Normalised voltage (-)
P^*	Normalised pressure (-)
Me	Average (-)
Sd	Standard deviation (-)
Sk	Skewness (-)
Ku	Flatness (-)

Abbreviations

CCFL	Counter-current flow limitation
PWR	Pressurized water reactor
SG	Steam generator
RPV	Reactor pressure vessel
PDF	Probability density function
PSDF	Power spectral density function
WE	Wavelet energy
DWT	Discrete wavelet transform
DPT	Differential pressure transducer
ZLP	Zero liquid penetration

Along with its importance in multiphase flow systems, including counter-current flow in the hot leg PWR, flow regimes' identifications have been widely studied. They engage the analysis of both subjective and objective methods. The subjective method may be mainly on the basis of the close visual observations (Mayinger et al., 1993; Wongwises, 1994; Choi & No, 1995; Zapke & Kröger, 1996; Ghiaasiaan et al., 1997; Petritsch & Mewes, 1999; Deendarlianto et al., 2008; Prayitno et al., 2012; Vallée et al., 2012a; Vallée et al., 2012b). On the other hand, the objective method pays attention more into the interfacial behaviors of the flow which can be revealed utilizing signal characteristics. It may contain resistive-conductance, capacitive, and also impedance signal characterizations. Earlier, an instantaneous liquid film thickness measurement and calibration on the basis of the resistivity conception was proposed by Koskie et al. (1989). It assessed two wires which were positioned both parallel to each other and normal to the liquid flow. The radial wire distance was controlled by two holes that were accurately positioned. The results reveal that the increase of Reynolds number affects the amplitude of the signal fluctuations even though they are taken under the same flow condition. Furthermore, the use of parallel-wire probes based on the electrical resistance principle to measure the liquid level in a geometry representing 1/15 hot leg PWR was reported by Kinoshita et al. (2011). A set of platinum wires with 0.1 mm of diameter was applied as the probe. A cumulative probability density function (PDF) was assessed to define the average liquid level on the basis of time-domain analysis. Moreover, the measurement accuracy of the parallel-wire array probe was successfully improved to measure water hold-up in near horizontal oil-water two-phase flow (Zhou et al., 2020). Here, the slip characteristics under certain flow regime were examined on the basis of quick closing valve method. The more recent investigation of slug flow pattern involving statistical characterizations in a horizontal conduit with 26 mm of the inner diameter applying resistive probe signals was carried out by Rodrigues et al. (2020). Such statistical analyses were developed to support the particular signal fluctuation behaviors. A PDF was assessed on the statistical characterization of the void fraction which was taken from five series of probes. They reported that the PDF strongly depends on the flow patterns. The higher the void fraction, the larger area of the peak on the PDF. Furthermore, under a given gas flow, as the liquid flow gradually increases, the peak indicating a lower void fraction is in its position while the right peak decreases in both its elevation and void fraction. On the other hand, under a given liquid flow rate, as the gas flow gradually increases, the left peak was similar to the previous, but the right peak shows an increase in void fraction.

The characterization of flow patterns on the basis of the time-series analysis was successfully investigated by Jin et al. (2003) using ring-type measuring electrodes. The results reveal that non-linear analysis of the conductance probe signal fluctuations

strongly indicates the flow pattern behavior, in which the Kolmogorov entropy (KE), representing the unpredictability level of the signals, increases with the gas flow. Another investigation on the counter-current flow regimes using conductance probe signals and artificial neural networks was developed by Ghosh et al. (2012; 2013). Such key factors governing the flow patterns were the flow rate, physical properties of fluids, diameter, and orientation of conduit. The results show that flow regimes affect all the transportation processes, i.e. the momentum balance, heat, and mass transfer (Ghosh et al., 2012). Moreover, further automatic classifier system was also developed by capturing the hydrodynamic characteristics through the objective description (Ghosh et al., 2013). Two types of conductance probes, i.e. the parallel-wire and ring conductance, had been utilized for this purpose. The clusters of flow regimes were established on the basis of the probe signal features using two classifiers separately. The most recent, analysis of flow structures using conductivity probe signals of liquid-liquid counter-current two-phase flow was reported by Samal & Ghosh (2021). The obtained results indicate that the observed flow structures have strong effects on both magnitude and fluctuation of the signals acquired.

The flow patterns determination on the basis of the characteristics of frequency-domain analysis by using power spectral density function (PSDF) of the capacitance probe signal was reported by Canière et al. (2007). They obtained that the stratified flow contributes to low frequency due to the slow fluctuations at the interface. In wavy flow, the higher frequency occurs due to waves in the interface. In slug flow, the dominant frequency occurrence is the liquid slug frequency. The annular flow usually has a contribution to the high frequency due to the turbulent structure of the interface caused by the high gas flow rate in the core. A further study on the slug flow in a horizontal conduit with 5 m on the length and 34 mm of diameter using capacitance probe signal was carried out by dos Reis & Goldstein (2010), while an assignment on flow regime clustering on the basis of the wavelet analysis of capacitance probe signals was successfully conducted by De Kerpel et al. (2015). Here, advanced diagnostic statistical tools were also utilized in the analysis. The wavelet variance was assessed to test the flow behaviors. The Daubechies 4 (db4) maximal overlap discrete wavelet transform was used to decompose the signals, while the Fuzzy c-means algorithm was utilized for flow regimes clustering. For further optimization and reducing the dimensionality of the feature space which were chosen manually, main component and linear discriminant analyses were also assessed. The data were divided into different clusters utilizing the c-means Fuzzy algorithm.

On the basis of time-frequency domain analysis, a two-phase flow patterns identification using the wavelet analysis of the void fraction data was proposed by Nguyen et al. (2010). An advanced signal analysis tool, i.e. a continuous wavelet transform (CWT)

with Debauchies order 4 (db4) was assessed to investigate the characteristics of the void fraction. The CWT analysis gave a local wavelet energy (LWE) coefficient, hence the LWE can be mapped, and various flow patterns were established. Under the flow pattern of slug flow, the LWE map shows that each peak of the void fraction has an elliptical shape which stretched from the smallest to the largest scale, and its size tends to consistent on each peak. Meanwhile, under the condition of a turbulent-churn flow, the LWE map tends to have an elliptical shape with various sizes on the peak of the void fraction. On the other hand, utilization of the parallel wire probes which was verified by wall mounted conductivity probes, Jana et al. (2006) successfully identified two-phase flow regimes by the energy fluctuations obtained by discret wavelet decompositions. Here, the passing droplets and wavy interfaces characterizations were obtained due to both the flow parameters i.e. liquid and gas superficial velocity, respectively.

The signal analysis on gas–liquid flow pressure fluctuations currently was successfully investigated by Hudaya et al. (2019). The liquid wave characteristics on the co-current horizontal stratified two-phase flow were obtained. Moreover, the interfacial behaviors of the sub regimes obtained by differential pressure fluctuations were identified throughout several advanced statistical tools involving time-domain, frequency-domain and also time–frequency domain analyses (Wijayanta et al., in press). Meanwhile, during the counter-current flow in a 1/3 scaled-down test facility of a PWR hot leg, the slug frequencies obtained by pressure probes was also reported by Lucas et al. (2017). Both authors utilized the fast Fourier transform (FFT) in order to determine either the dominant wave or the slug frequencies. Furthermore, the pressure fluctuations during the flooding regimes have been investigated by Astyanto et al. (2021b). A test section with a 25.4 mm of inner diameter representing 1/30 hot leg PWR geometry was utilized. Moreover, three riser length to diameter (L_r/D) ratios were also utilized to investigate the effect of the riser length on the pressure signal fluctuations (Astyanto et al., 2021a). In addition, an advanced observation during characterization of flow structure on airlift pump-bubble generator system using the pressure differential signal was reported by Catrawedarma et al. (2021a). Two test sections containing the top section and bottom section were assessed. The Kolmogorov entropy was used to measure the degree of unpredictability. The result indicates that the increase of entropy corresponds to the increase of the gas flow. However, under a specified gas flow rate, the entropy tends to stagnate in further increments. Moreover, the energy distributions were utilized as the inputs on flow regime clustering by means of artificial neural network (Catrawedarma et al., 2021b).

During its milestone, the studies in counter-current two-phase flow have been carried out in various platforms of analytical studies, mathematical modellings, finite volume based computations, and also mechanistic modelling on the basis of experimental investigations. Several importance parameters investigated contain the conduit geometries (diameter, horizontal length to diameter L_H/D ratio, inclined length to diameter L_I/D ratio), the complexity of the configurations, the cross sectional area shapes (rectangular, annuli, circular), the channel orientations (horizontal, vertical, incline), the entrance and exit geometries, and also the fluid physical property effects (viscosity and surface tension). Moreover, the experiments in the complex geometry representing a PWR hot leg have been conducted in various model of scales. Based on scientific review reported by Deendarlianto et al. (2012) and Al Issa & Macian-Juan (2011), the use of full scale model (with a 750 mm of inner diameter) were investigated by Mayinger et al. (1993), and Glaeser & Karwat (1993). On the other hand, scale of 1/3 and 1/3.9 were carried out by Deendarlianto et al. (2008), Vallée et al. (2012a), Lucas et al. (2017) and Al Issa & Macian-Juan (2014), Al Issa and Macián-Juan (2017). The scale of 1/15 was reported by

numerous authors i.e. Ohnuki (1986), Navarro (2005), Minami et al. (2010), and also Vallée et al. (2012b). From those studies it was revealed that the data error is still observed (Deendarlianto et al., 2012). In addition, a reduced-size representing a small scale reactor is also investigated in its development in order to enhance the experimental database. Although the 1/30 was not carried out as many as 1/15, this scale was reported by Ohnuki (1986), and Badarudin et al. (2016), Badarudin et al. (2018a), Badarudin et al. (2018b).

From the above facts, it is noticed that the signal processing is able to investigate the flow structures. However, experimental studies on the characteristics of counter-current flow structure which utilizes an advanced signal processing tools in the complex geometry containing a horizontal and inclined pipe connected by an elbow which represents a hot leg of a PWR remain less attention. Therefore, the present work attempts to conduct the statistical characterizations of the liquid film obtained from resistive-conductance probe signals during the counter-current flow on a small-scale reactor. Several pairs of parallel-wire array probes are embedded to elaborate the interfacial behaviors of the liquid–gas two-phase countercurrent flow with respect to the location along the horizontal part of test section representing a 1/30 down-scaled of a PWR hot leg. Furthermore, some advanced statistical diagnostic tools are applied to describe the interfacial behaviors through the characteristics of the liquid film thickness fluctuations. The obtained results will contribute to enrich the database in order to develop a mechanistic model to predict the CCFL.

2. Experimental apparatus and procedures

A schematic diagram of the apparatus used in the present experimental study is shown in Fig. 1(a), while the physical properties of the working fluids are tabulated in Table 1. The experimental apparatus has been constructed at the Laboratory of Fluid Mechanics, Department of Mechanical and Industrial Engineering, Universitas Gadjah Mada. Moreover, the test section employed in this work is shown in Fig. 1(b). It is a complex geometry containing a horizontal and an inclined conduits connected by an elbow which represents a 1/30 down-scaled of PWR hot leg Germany-KONVOI. The test section was made from transparent acrylic resin to enable close visual observations of the flow structures and phenomena. The cross-sectional area is circular with an internal diameter of 25.4 mm, while the lengths of the horizontal section, the inclined length (riser), and the inclination angle of the riser are 635 mm, 100 mm, and 50°, respectively. Moreover, the SG and RPV simulators were made from transparent-flat acrylic with 22 cm × 13 cm × 32 cm, and tempered glass with 22 cm × 22 cm × 72 cm, both in length, width, and height. In addition, the scaling of the test section and geometries of the main supporting components were utilized by Badarudin et al. (2016, Badarudin et al., 2018a; Badarudin et al., 2018b) during the investigations of both the geometrical effects and interfacial phenomena on gas–liquid two-phase countercurrent flow.

In the present work, a pair of air–water based fluid (aquadest +40% glycerol) was used as the working fluids. Here, a nondimensional Wallis parameter was applied to determine both the liquid and gas superficial velocity range, since it was reported that the fluid combination does not affect to the relationship between the nondimensional Wallis parameter (Ohnuki, 1986). The range of the liquid discharge is 2–48 gallons per hour (gph). However, since the flowmeters used are water flowmeters, a correction was carried out in order to obtain the actual/corrected volumetric flow rate. Moreover, a curve representing the onset of flooding was utilized due to the verification of the determined flow parameters. Here, as shown on the Fig. 2, the obtained result shows that in

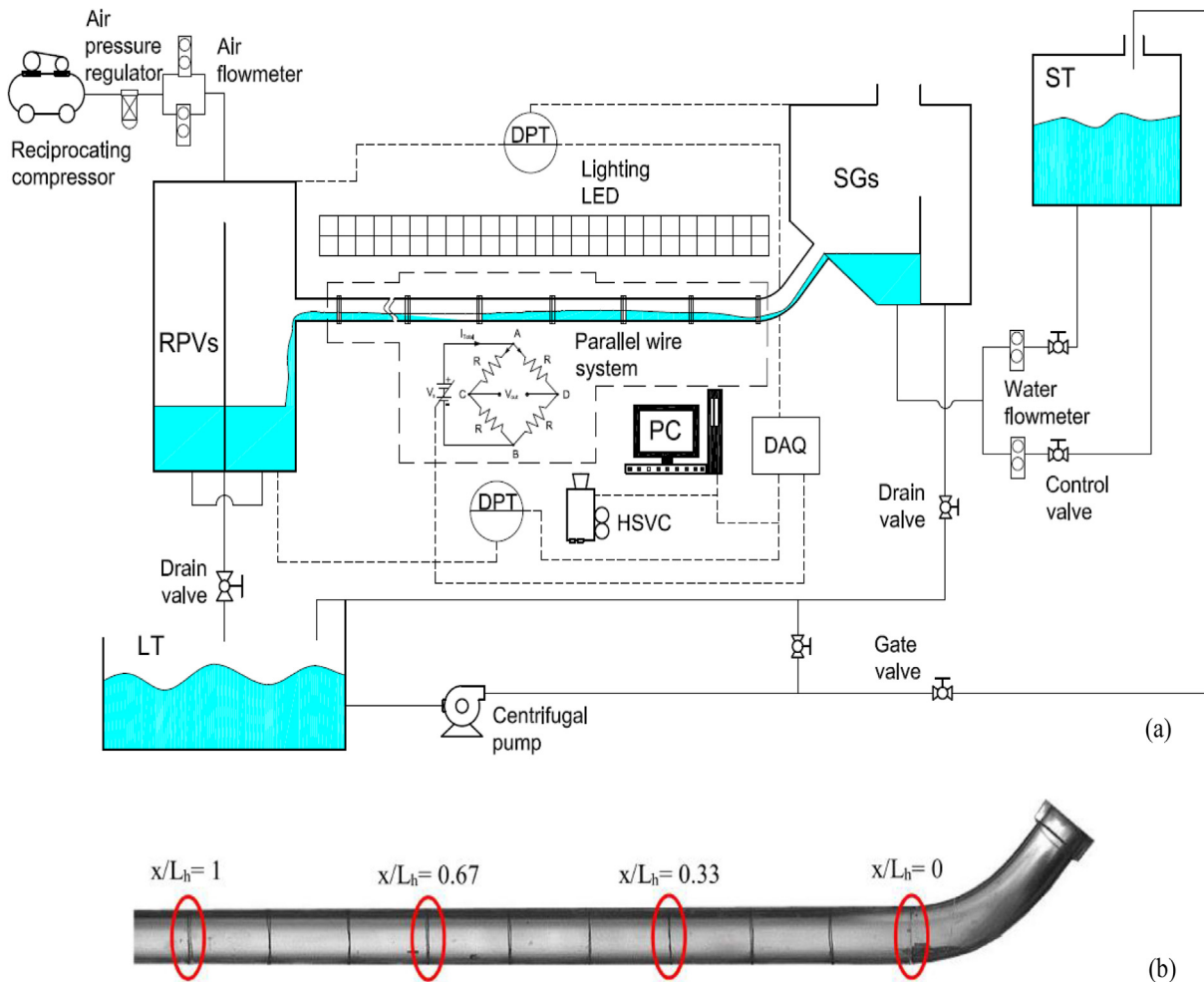


Figure 1. (a) Schematic diagram of experimental apparatus; (b) Test section.

Fig. 1. (a) Schematic diagram of experimental apparatus; (b) Test section.

Table 1
Fluids physical properties.

Physical properties	Aquadest + 40%wt glycerol	Air
Fluid density at 30 °C (kg/m ³)	1074.63	1.165
Surface tension (N/m)	0.056	-
Dynamic viscosity at 30° C (kg/m. s)	3.34×10^{-3}	1.87×10^{-5}

agreement with Navarro (2005), Vallée et al., (2012a) and also Kinoshita et al. (2011), the gas flow rate that initiates flooding decreases with the increases of the liquid flow rate.

Moreover, during the selected flow parameters involve both the liquid and gas volumetric flow rates as shown in Table 2. The tests were conducted under the atmospheric pressure. Thanks to the method, due to its convenience as a non-dimensional parameter, the Wallis parameter could be taken into account to correlate CCFL data during the effect of density ratio. Here, it was previously reported that the fluid combination does not affect to the relationship between the nondimensional Wallis parameter during a theoretical approach (Ohnuki, 1986). This fact is then supported by several others experimental investigations as reported by Deendarlianto et al. (2008) and also Van Ommen et al. (2011) during air/water experiments. Deendarlianto et al. (2008) carried out

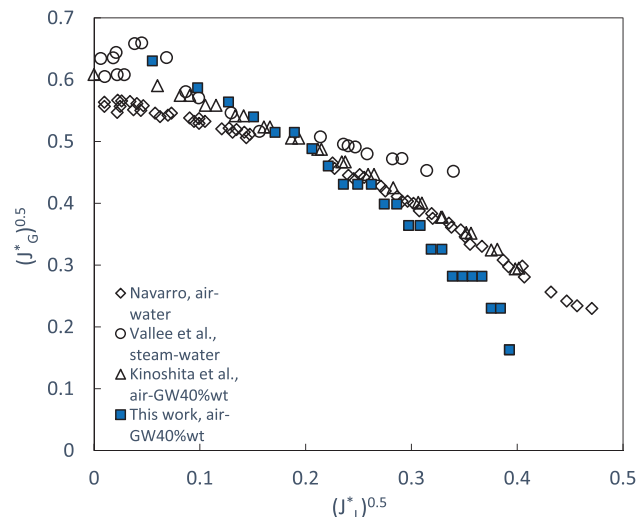


Fig. 2. Wallis parameter comparison during the liquid flow rate range determination.

Table 2
Test matrix.

System pressure (bar)	1					
Corrected liquid flow rates (gph)	3.9		8.6		13.4	
Corrected gas flow rates (lpm)	1	97.6	1	85.4	1	61
	2	109.8	2	97.6	2	73.2
	3	122	3	109.8	3	85.4
	4	134.2	4	122	4	97.6
	5	146.4	5	134.2	5	109.8

the experimental study using a 1/3 model of PWR hot leg to investigate the influence of system pressure on the CCFL. They reported that since the air density affects the air pressure, in which a higher density of the air corresponds to higher air pressure, then the higher the system pressure, the higher the air flow needed to initiate flooding, and vice versa. However, it is also notified that to changes the system pressure from 3 to 1.5 bar, the interfacial behaviors during the CCFL are almost the same. Therefore, the film thickness fluctuations may have the similar trend.

In addition, in the scientific report by [Deendarlianto et al. \(2012\)](#), it is noticed that the scaling through Wallis parameter is able to correlate the CCFL data. Here, from an analytical work carried out by [Gleaser \(1992\)](#), it was found also that the Wallis parameters which was initially proposed during vertical countercurrent flow can be applied for the CCF in a horizontal large conduit. Furthermore, during the experiment comparison between air/water and steam/water, [Vallee et al. \(2012\)](#) reported that over a wide range of both pressure and temperature conditions, the Wallis similarity is appropriate to scale the flooding. Moreover, [Lucas et al. \(2017\)](#) successfully elaborated another insight to what previously reported by [Vallee et al. \(2012\)](#) during HZDR projects compliance. Here, the flow structure is successfully investigated in which the higher the pressure, the larger the slug frequencies. From the aforementioned works, the authors presumed that applying the Wallis parameter to ensure that both the determined gas and liquid flow rates' range are then appropriate.

The working procedure of the experimental apparatus is briefly explained as follows. An amount of liquid from the liquid container (LT) was pumped by a centrifugal pump into the storage tank (ST). Due to gravitational force, liquid flows downward through two parallel conduits. In this part of the section, a 20 gph with a 2 gph of scaled measurement range of water flowmeter and a control valve are installed with each conduit. As time proceeds, liquid moves to the upper tank which represents the steam generator simulator (SGs), flows along the hot leg into the lower tank as the reactor pressure vessel simulator (RPVs). Meanwhile, air from a reciprocating compressor with constant pressure which is maintained by an air pressure regulator with a maximum working condition of 10 bars, flows through the airflow meter enclosed with a flow rate tuner. Next, the air moves into the RPVs, then flows along the hot leg counter-currently with the liquid into the SGs and is released to the atmosphere.

The carried-out measurements engage the pressure fluctuations in the RPVs, and also the liquid film fluctuations in the horizontal section. Types and specifications of those instruments are orderly listed in [Table 3](#). Moreover, the pressure fluctuations were acquired using differential pressure transducers (DPT). Here, a unit of Validyne P55 series with a measurement range of 86 kilo Pascal (kPa) for the RPVs air pressure measurement was allocated. On the other hand, a measurement line during the RPVs water level determination was also utilized. It was validated by time-series static pressure fluctuations. For this reason, another Validyne P55 series with a 54 kPa of measurement range was employed. Those two pressure transducers were empowered by a 12 VDC power supply.

Table 3
Typical instrumentation and specifications.

Instrument	Type	Specifications
Gas flowmeter	Dwyer RMA	0–70 lpm (4% measurement accuracy)
Liquid flowmeter	Dwyer RMB	0–20 gph (3% measurement accuracy)
DPT	Validyne P55D	86 kPa (0.25% measurement accuracy)
	Validyne P55D	54 kPa (0.25% measurement accuracy)
DAQ	Advantech 4716AE	200 kS/s; 16-bit; 16 channels
HSVC	Phantom Miro LAB310	3200 fps at 1280 × 800 pixel (maximum resolution)

Several pairs of parallel-wire conductance array probes were applied to obtain the time-series of liquid film thickness fluctuations along the horizontal part of the test section. This typical probe was previously investigated as one of the effective probe during objective flow regime identification by [Ghosh et al. \(2012\)](#), whereas the conceptual analysis of the probe was described by [Koskie et al. \(1989\)](#), and also [Zhou et al. \(2020\)](#). In the present work, the nickel wires with a diameter of 0.5 mm and a gap of 5 mm apart were positioned normal to the fluid flow with a distance of 20 mm each along the horizontal part of the test section. Those probes were connected to an in-house-fabricated Wheatstone bridge module to enhance its sensitivity as previously was also applied by [Jana et al. \(2006\)](#), [Kinoshita et al. \(2011\)](#), [Ghosh et al. \(2012; 2013\)](#), [Badarudin et al. \(2018a\)](#), [Badarudin et al. \(2018b\)](#), and also [Samal & Ghosh \(2021\)](#). To obtain a simultaneously analog to digitalize data acquired between the time-series of the pressure, water level, and also the liquid film thickness fluctuations, those pressure transducers, and parallel-wire probes were connected to a 200-kS/s 16-bit and 16-channels Advantech 4716AE data acquisition (DAQ) system with a sampling rate of 1000 samples per second. The utilization of this sampling rate was also previously reported by [Kinoshita et al. \(2011\)](#), [Catrawedarma et al. \(2021a\)](#), [Catrawedarma et al. \(2021b\)](#), and [Samal and Ghosh \(2021\)](#) in their works. Furthermore, 15 s period of data acquired was applied during its tabulation as previously was also utilized by [Catrawedarma et al. \(2021a\)](#), [Catrawedarma et al. \(2021b\)](#). Here, the maximum point of frequency which was below 10 Hz was taken into the consideration during the determination as also previously reported by [Johnsson et al. \(2000\)](#), and [Van Ommen et al. \(2011\)](#). Since the dominant frequency of signal fluctuations was below 10 Hz, 10 s of time-sampling obtained a necessary duration.

Moreover, a set of high-speed video cameras (HSVC) was used. Here, a Phantom Miro LAB310 with a recording rate at 60 frames per second and 1280 × 720 pixel of resolution was applied. Furthermore, all the data acquired including the parallel wire probes, the pressure fluctuations, and the camera recordings were stored on a personal computer (PC). In addition, the wavelet signal analysis utilizes the MATLAB toolbox, while both the time-domain and the frequency-domain analyses including the PDF, PSDF, and

also the Kolmogorov entropy calculation were developed on the basis of the MATLAB programming language.

3. Results and discussions

3.1. Flow visualization

Fig. 3 shows the flow development during the counter-current flow under the liquid superficial velocity (J_L) of 0.028 m/s. From the figure, it is noticed that under the gas superficial velocity (J_G) of 2.41 m/s, a stable countercurrent flow which is characterised by a constant and low pressure drop as depicted in Fig. 4 is detected. Here, a thin liquid film, which is called supercritical flow, is observed from the riser downward to the elbow. On the other hand, another thick liquid film, which is called subcritical flow, occurs at almost the entire horizontal part. As a result, a hydraulic jump (HJ) is initiated at the bend as the transition from the supercritical to the subcritical region. Moreover, it enables the liquid velocity to exceed the gravity wave velocity which corresponds to the ratio of inertial towards gravitational force, called the Froude number (Siddiqui et al., 1986).

As time goes by, a stratified flow along the horizontal part of the test section is still observed when the gas flows counter-currently with the liquid at a slight increase of gas superficial velocity ($J_G = 2.81$ m/s). However, the increase of the gas flow rate leads to the retention of liquid by the gas. As a result, the liquid level in the horizontal part near the elbow at the upper end of the HJ also rises. Consequently, the HJ shifts near the bend, and a smooth-small wave is occasionally observed. This further phenomenon which corresponds to the interfacial friction force which increases with the increase of the gas flow was also previously reported by Deendarlianto et al. (2008), Deendarlianto et al. (2011) and also Badarudin et al. (2016; Badarudin et al., 2018a; Badarudin et al., 2018b). A further increase of the gas superficial velocity up to $J_G = 3.21$ m/s forms a liquid blockage which initiates the flooding in a certain probe location/locus (x/L_h) of the horizontal part and causes a sudden and drastic increase in the pressure difference

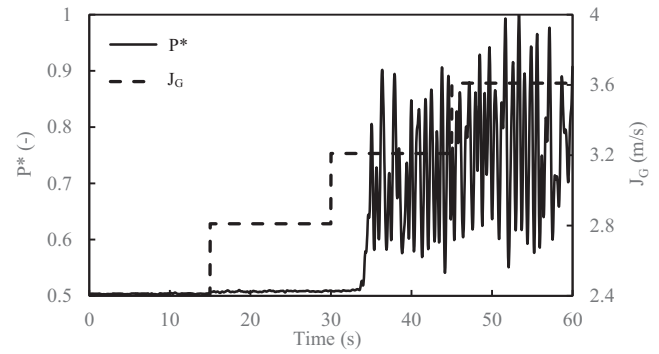


Fig. 4. Normalized pressure fluctuations under $J_L = 0.028$ m/s.

between the SGs and RPVs as shown in Fig. 4. This sudden fluctuations of the pressure difference corresponds to a phenomenon in which the blockage process by the liquid flow compresses the gas flow in the conduit and leads to the increase of the pressure and the occurrence of slug. Hence, it is also noticed that the rate of the liquid level in the RPVs decreases following the onset of liquid blockage as partial volume of liquid are entrained by the gas flow.

In addition, the flooding mechanism under these particular parameters ($J_L = 0.028$ m/s and $J_G = 3.21$ m/s) is further explained sequentially as depicted in Fig. 5. As time goes by, the liquid level in the horizontal part near the bend rises relative to time simultaneously. As a result, the liquid level increases until it leaves a narrow gap next to the HJ for the gas flow, followed by wavy interface along the HJ. As time progress, the wave grows and initiates the onset of liquid blockage at the thick end of the HJ. A similar blocking of the pipe cross sectional area by a wave growth was also reported by Deendarlianto et al. (2005), Deendarlianto et al. (2010) and also Ousaka et al. (2006) for the upper flooding mechanism during CCFL experiments in the inclined pipes. Furthermore, the first-occurring slug is followed by series of slugs with the larger sizes. The slugs which are formed in the position near to the riser

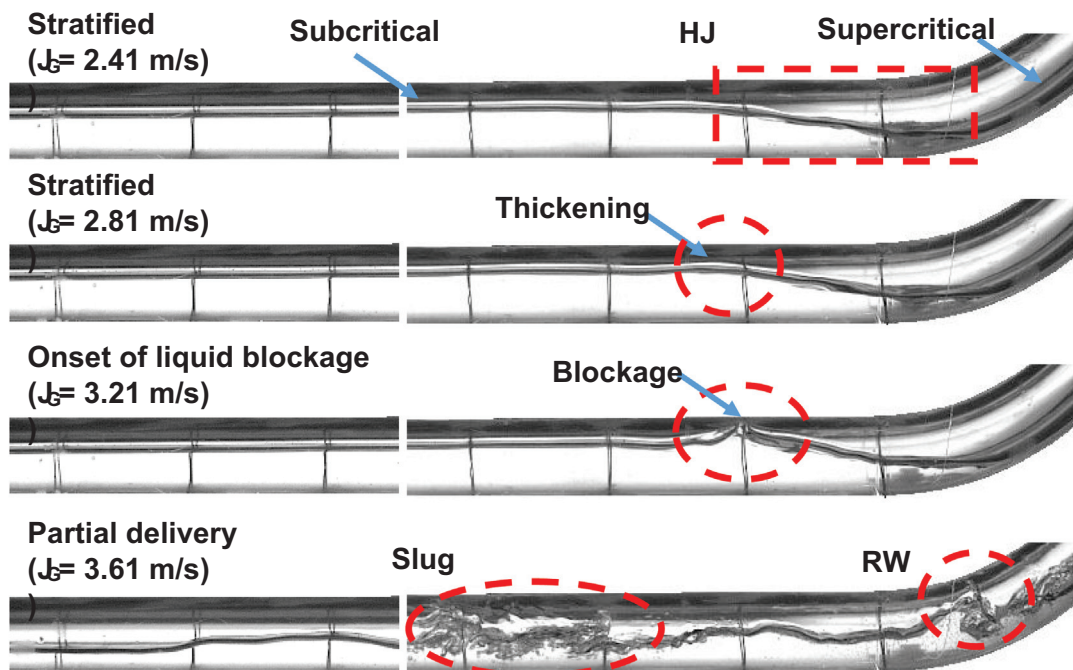


Fig. 3. Flow development under $J_L = 0.028$ m/s.

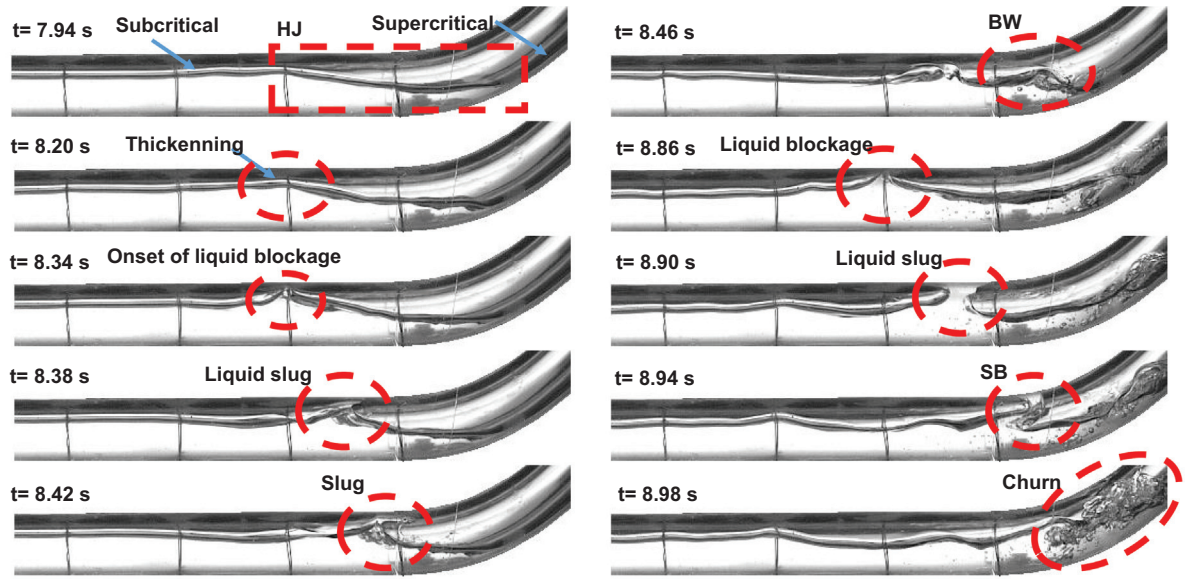


Fig. 5. Flooding mechanism under $J_L = 0.028$ m/s and $J_G = 3.21$ m/s.

eventually propagates to bend incrementally slug, until they reach the bend. However, it can also be observed that such air bubbles are also generated around the bend indicating a churn flow and moving upward after the bend to the riser. These phenomena are in good agreement with that of Vallée et al. (2012) who also confirmed that in bend, the slug formation involves bubble generation.

3.2. Stochastic analysis

Stochastic analysis has successfully been utilized to identify the flow pattern on the basis of the effect of flow rate both in vertical conduits (Jana et al., 2006; Ghosh et al., 2012, 2013) and horizontal pipes (Canière et al., 2007; dos Reis & Goldstein, 2010), both the wave frequency and liquid film distribution during the investigation on liquid viscosity's effect on horizontal annular flow (Setyawan et al., 2016; 2017), the submergence ratio on airlift pump micro-bubble generator system (Catrawedarma et al., 2021a; Catrawedarma et al., 2021b), and also conduit orientation effects on counter-current two-phase flow system (Samal & Ghosh, 2021). It enables the transformation of random time-series signals to accomplish the quantification terms of statistical moments namely standard deviation (Sd), skewness (Sk), and kurtosis (Ku) (Jana et al., 2006; Catrawedarma et al., 2021a; Catrawedarma et al., 2021b; Samal & Ghosh, 2021). Moreover, such flow characteristics i.e., the liquid thickness, also the presence of hydraulic jumps and waves, are able to be evaluated (dos Reis & Goldstein, 2010). In addition, such details for both time and frequency domain analysis on flow regime identifications in a two-phase flow was described by Johnson et al. (2000).

The power spectral density function (PSDF), describing the frequency-domain analysis of a signal through a fast Fourier transform (FFT), corresponds to the wave formation's occurrence which is implied by its physical frequency. Here, the dominant frequency is obtained by the highest magnitude of the frequency. Moreover, each segment of the power spectrum, estimated as a number of sub-spectra by reducing the signal variance, divides the time-series into L segments with individual lengths N_s as follows:

$$P_{xx}^i(f) = \frac{1}{N_s U} \left| \sum_{n=1}^{N_s} x_i(n) w(n) \exp(-j2\pi fn) \right|^2 \quad (3.1)$$

here in the Equation (3.1):

$$x_i(n) = x(n + iN_s) \quad i = 1, 2, 3, \dots, Ln = 1, 2, 3, \dots, N_s \quad (3.2)$$

In the function of window, $w(n)$, the normalized by the factor of power. Thus,.

$$U = \frac{1}{N_s} \sum_{n=1}^{N_s} W^2(n) \quad (3.3)$$

The averaged power spectrum is defined as:

$$P_{xx}(f) = \frac{1}{L} \sum_{i=1}^L P_{xx}^i(f) \quad (3.4)$$

In the present work, the statistical characterization of the signal fluctuations obtained by the PDF and PSDF is described in Fig. 6. Here, the flow condition was kept constant at $J_L = 0.028$ m/s. From the figure it is noticed that the lower gas flow rate results in comparatively smaller FFT values in the PSDF. However, a relatively small spectral magnitude and a dispersed peak distribution in around a large interval of frequency (1–50 Hz) indicates that a stratified regime is observed. A further increment in gas flow results the decrease of the dominant frequency in which the visual observation reveals that the occurring fluid flow is wavy. When the onset of liquid blockage is reached, the FFT magnitude increases significantly. The combination of PDF curve and the increase of the PSDF curve occurs simultaneously with slug flow in the test section. The detail investigation obtained from the experiment can be explained as follows.

As the gas flow increases from 2.41 m/s to 2.81 m/s, the fluctuations of the normalized voltage, V/V_{\max} , also increase as depicted in Fig. 6(i) and (ii). Here, the obtained time domain of the near-stable signal is shown in column (a). The distribution of the signals in this flow condition tends to produce a single-peaked (unimodal) PDF curve with negligible standard deviation as shown in column (b). This type of signal may correspond to the steady V/V_{\max} to a single point confirming the continuity of the liquid phase as also reported by Jana et al. (2006). Moreover, a shifting of the maximum frequency in the PSDF curve to a lower FFT magnitude as shown in column (c) is also captured. In addition, from Fig. 6(ii) and (iii), it is visible that the FFT magnitude of the signal fluctuation increases by two orders of magnitude as the gas flow is increased from 2.81 m/s to 3.21 m/s. Here, the time domain of signals is obtained partially fluctuating as shown in column (a) and followed by the

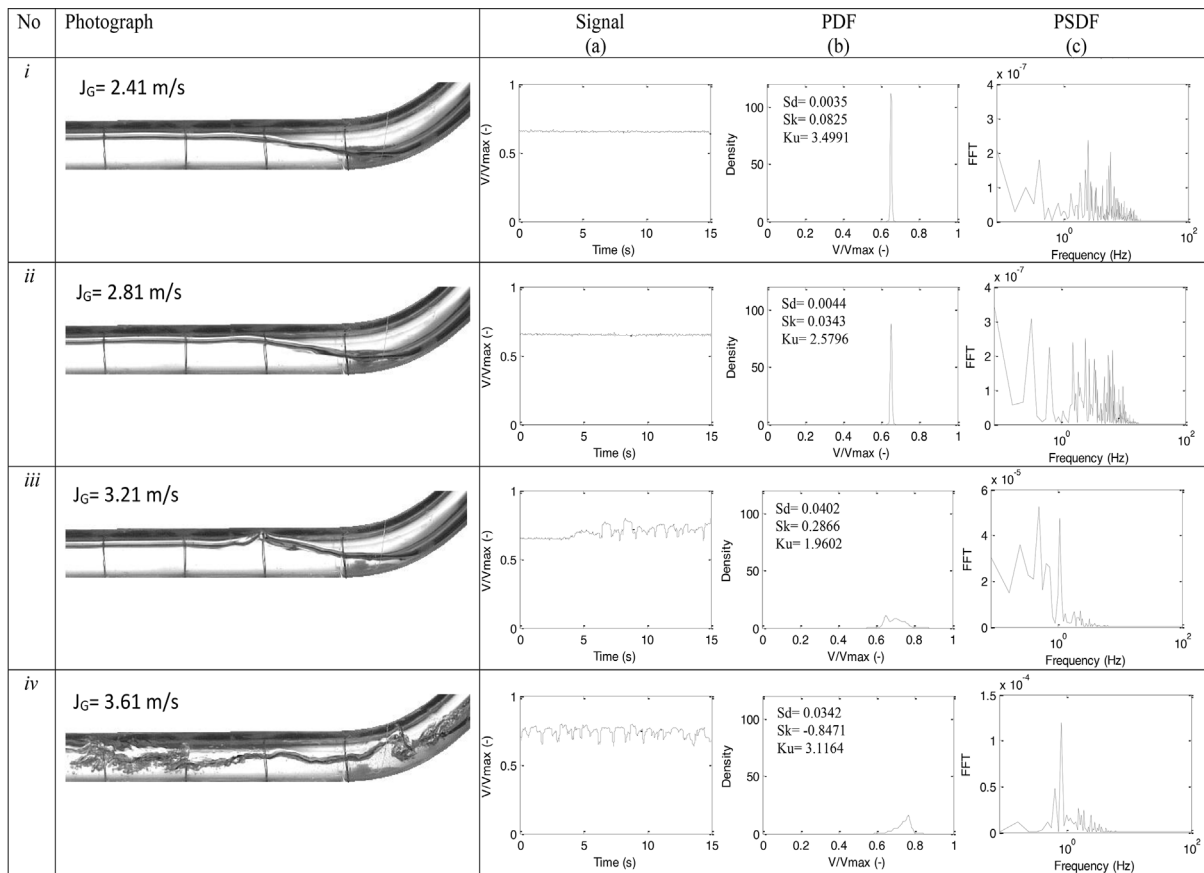


Fig. 6. Typical of signal fluctuations' statistical characterization under $J_L = 0.028$ m/s and various gas discharges at $x/L_h = 0.33$.

shifting of maximum point to a higher frequency as shown in column (c). Furthermore, in Fig. 6(iii) and (iv) the amplitude of the signal fluctuation increases further as the gas flow was increased from 3.21 m/s to 3.61 m/s. Here, the time domain of the signal fluctuates as shown in column (a) followed by the shifting of maximum point to a higher frequency as shown in column (c). Another shifting from positive to negative skewness probably reveals a smooth change in the interface.

Generally, before the onset of liquid blockage, the PDF depicts a single-peaked curve. It corresponds to a specific value of the normalized voltage which indicates that the fluid flow tends to stay at a certain void fraction. This behavior indicates that a stratified flow or a wavy flow behavior occurs, in which the latter is differentiated by the larger width of the curve relative to the former. When the onset of liquid blockage is reached, the PDF gives a multi-peaked (multimodal) curve, which indicates that more than one void fractions appeared significantly. The peaks in the lower end of the curve correspond to the lower void fraction values, while the higher end corresponds to higher void fraction values, suggesting a liquid slug flow was occurring (Rodrigues et al., 2020).

The statistical characterization of the signals under the flow condition of $J_L = 0.028$ m/s and $J_C = 3.21$ m/s for various locus is orderly depicted in Fig. 7. From the figure, it can be implied that the fluctuation of the normalized voltage, V/V_{max} , decreases along with the position shifts closer to the liquid exit (RPVs). Here, the time domain of the signal obtained visibly fluctuates as shown in column (a), which probably corresponds to the transition from stratified to slug flow through the visual observation. Furthermore, the distribution of the signals tends to widen with multiple peaks

as depicted in column (b) without shifting of maximum point to both the lower and higher frequency as shown in column (c).

Fig. 8 shows the effect of the gas flow on the statistical characterization of a given liquid flow rate of 0.028 m/s. From the figures, it can be obtained that a low gas flow rate where the flow regime observed is stratified, the signal fluctuation tends to decrease along with the location shifts closer to the liquid exit. Physically, the increase of the liquid level in the horizontal part of the test section corresponds to the decrease in the voltage reading on the data acquisition. When the gas flow rates are 2.41 m/s and 2.81 m/s, respectively, the normalized voltage decreases at all probe locations.

The statistical characterization as the function of the liquid superficial velocity is described in Fig. 9. As shown in the figure, under a constant of $J_L = 0.012$ m/s, the normalized voltage shows a value around 0.7 as depicted in Fig. 9(i). Here, the time domain of the near-stable signal is shown in column (a). The distribution of the signals under this flow condition tends to produce a single-peaked (unimodal) PDF curve with negligible standard deviation as shown in column (b). This typical signal may correspond to the steady V/V_{max} to a single point confirming the continuity of the liquid phase. As the liquid superficial velocity increases from 0.012 m/s to 0.025 m/s, the fluctuation of the normalized voltage decreases as depicted in Fig. 9(i) and (ii). Here, the time domain of the near-stable signal is shown in column (a). The distribution of the signals in this liquid flow rate also tends to produce a unimodal PDF with negligible standard deviation as shown in column (b). This typical signal still corresponds to the steady V/V_{max} to a single point which confirms the continuity of the liquid phase. A

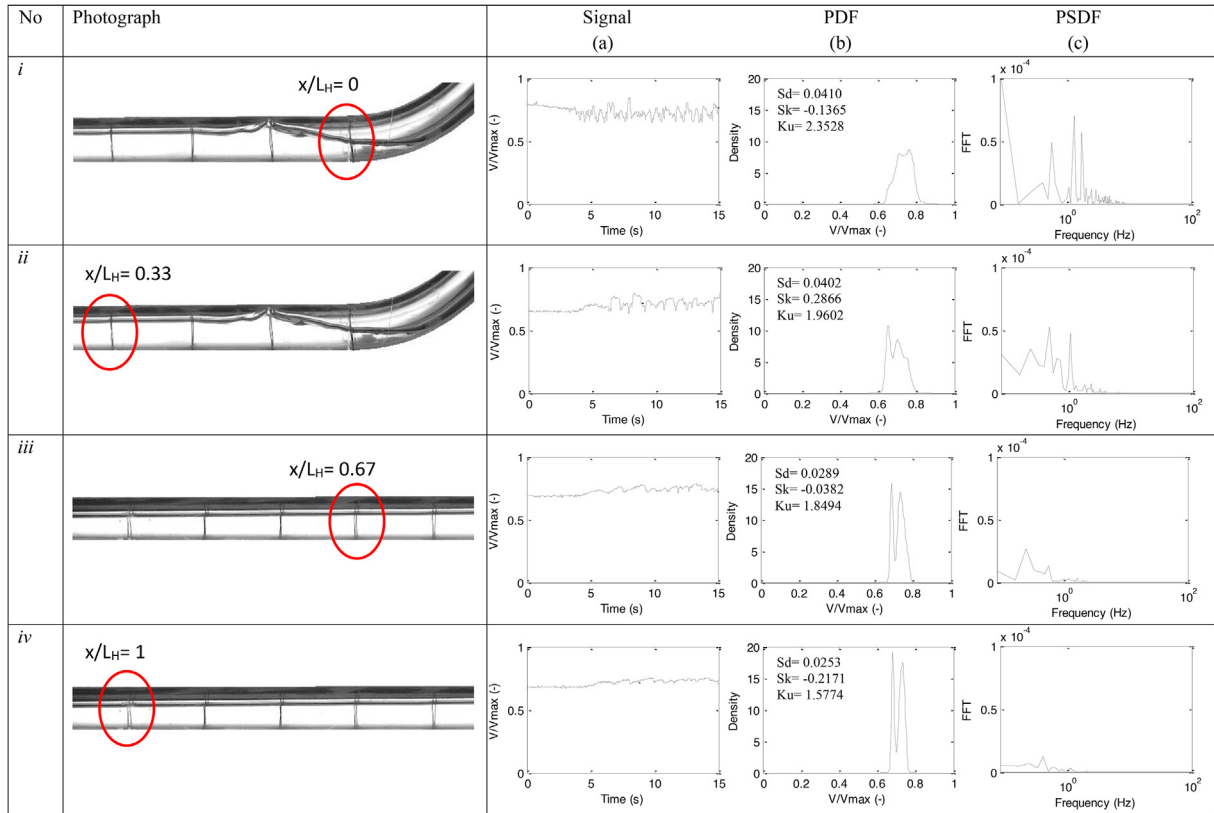


Fig. 7. Typical of signal fluctuations' statistical characterization under $J_L = 0.028$ m/s and $J_C = 3.21$ m/s at various probe locations.

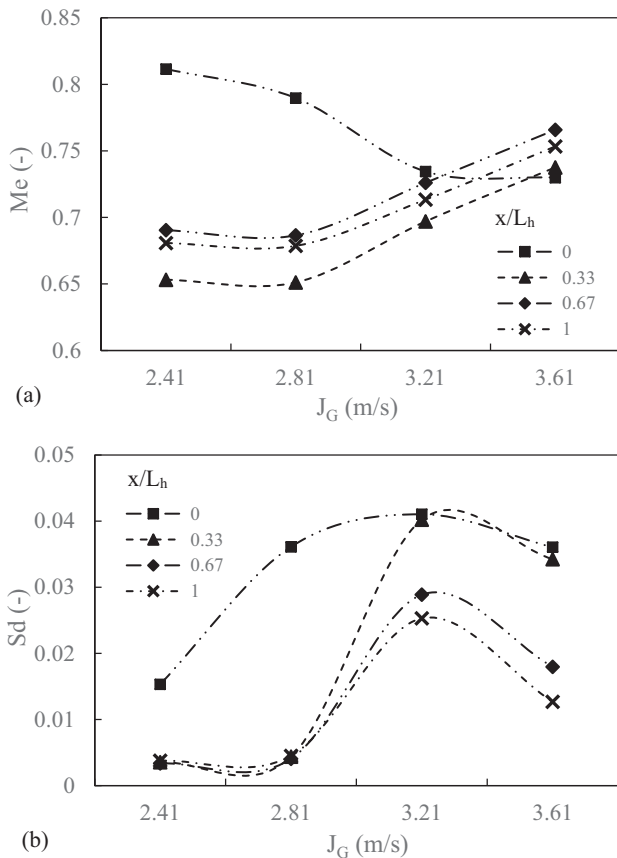


Fig. 8. The effect of gas discharges on (a) average; (b) standard deviation data under $J_L = 0.028$ m/s at various probe locations.

shifting from positive to negative skewness probably also reveals a smooth change in the interface. Moreover, a shifting of the maximum frequency in the PSDF to a lower FFT magnitude as shown in column (c) is also clearly captured. Furthermore, in Fig. 9(ii) and (iii) the amplitude of the signal fluctuations increase further as the gas flow was increased from 0.025 m/s to 0.028 m/s. Here, the time domain of the signal fluctuates as shown in column (a), and followed by the shifting of maximum point to a higher frequency as shown in column (c).

Fig. 10 shows the effect of the liquid flow on the statistical characterization under a constant of $J_G = 3.61$ m/s. From the figure, it is observed that at low liquid flow rates in which the observed flow regime is stratified, the signal fluctuation tends to decrease along with the location shifts closer to the liquid exit. When the liquid superficial velocity is increased from 0.012 m/s to 0.023 m/s, the normalized voltage decreases at all probe locations. On the other hand, the increase of liquid flow will increase the normalized voltage, except for the investigation locus near the bend.

3.3. Chaotic analysis

A chaotic analysis describes the unpredictability level of a system. The experimental deterministic chaos from a time-series signal can be characterized by its Kolmogorov entropy as earlier proposed by Grassberger & Procaccia (1983). Moreover, it can detect the flow transition points (Zhang et al., 2010). The entropy, measuring the loss information along the attractor, may be expressed in bits/s to relate the average cycle time and reflects it in real time unit (Johnsson et al., 2000). It also correlates to the signal characteristics obtained by the PSDF (Jin et al., 2003). In addition, the details of chaotic analysis on flow regime identification in a two-phase flow were described by Jin et al. (2003), and also Zhang et al. (2010).

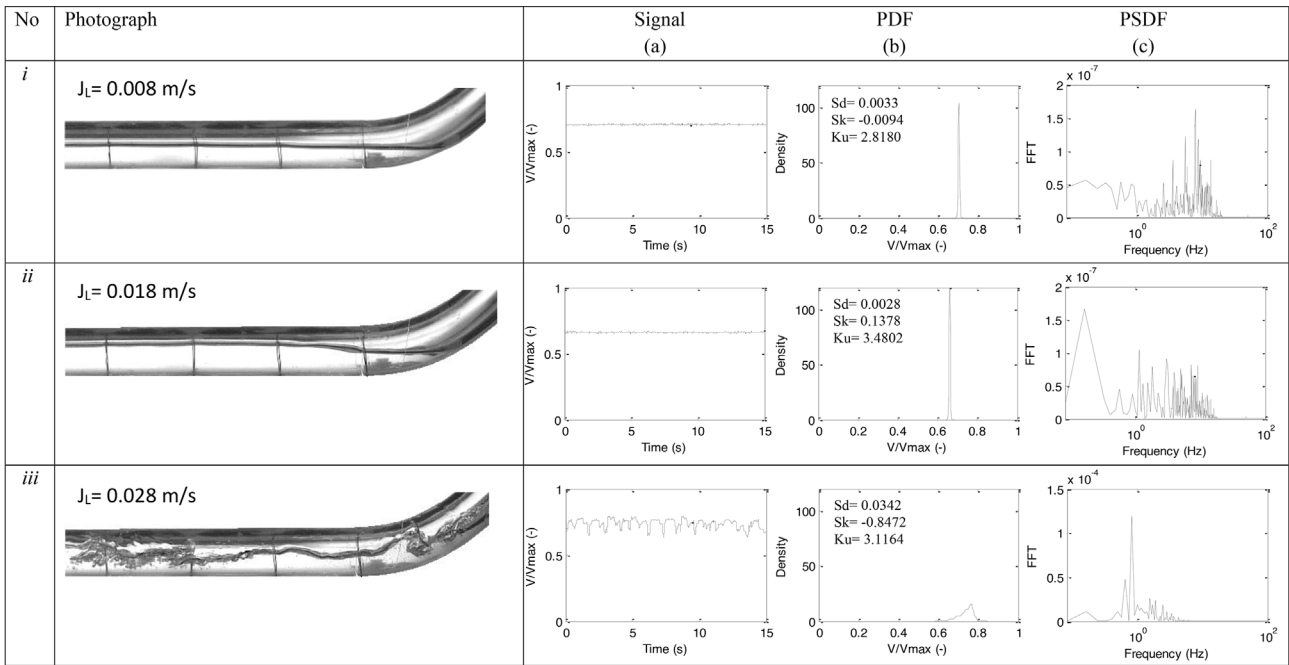


Fig. 9. Typical of signal fluctuations' statistical characterization under $J_G = 3.61$ m/s and various liquid discharges at $x/L_h = 0.33$.

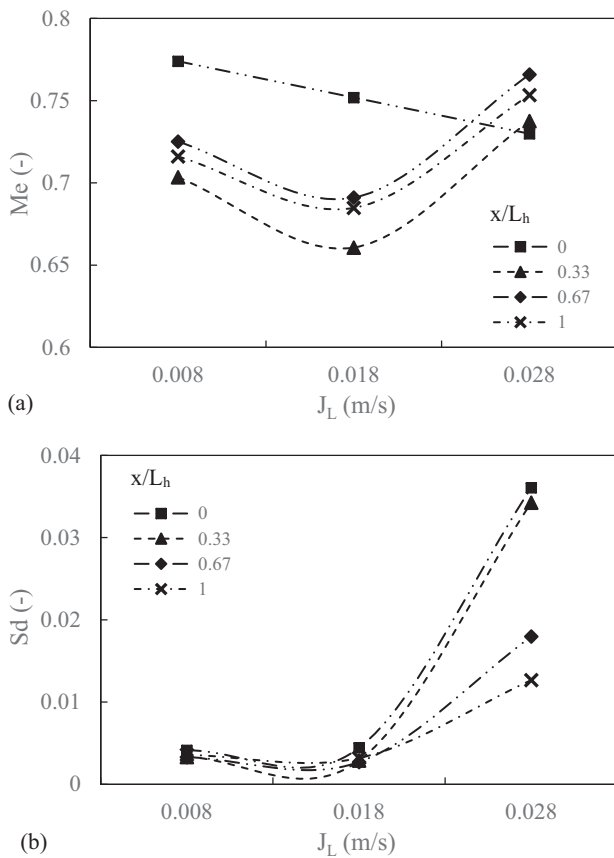


Fig. 10. The effect of liquid discharges on (a) average; (b) standard deviation data under $J_G = 3.61$ m/s at various probe locations.

In the present study, the entropy analysis towards specified wire sensors with various gas flow rates is shown in Fig. 11(a). It can be inferred from the figures that the flow entropy tends to fluctuate with the increase of gas flow. Here, the flow entropy

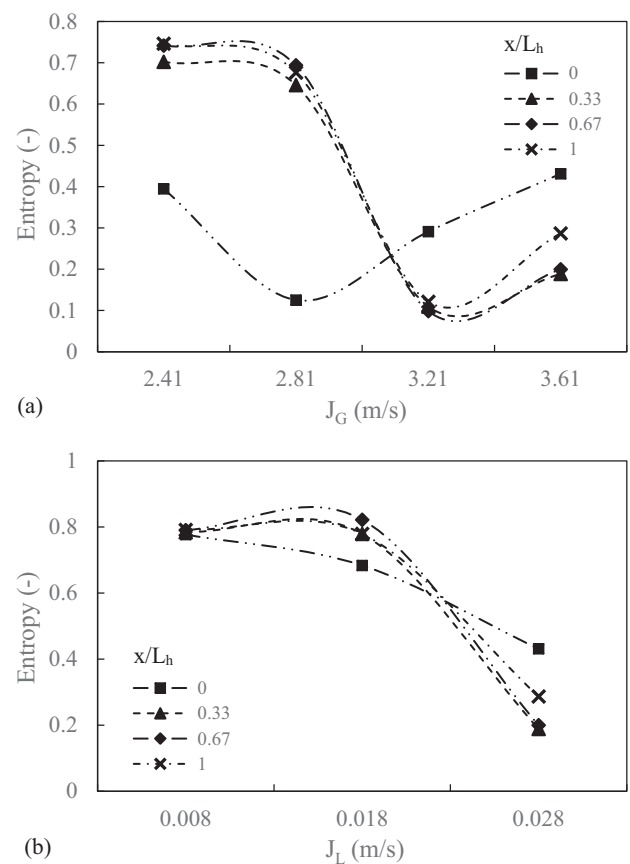


Fig. 11. The effect of (a) J_G , and (b) J_L on entropy data at various probe locations.

decreases with the increase of gas flow until the onset of liquid blockage is reached. On the other hand, a further increase of the gas flow after the onset of liquid blockage (PDR) causes an increase in the entropy for all sensor positions. This fluctuation trend in

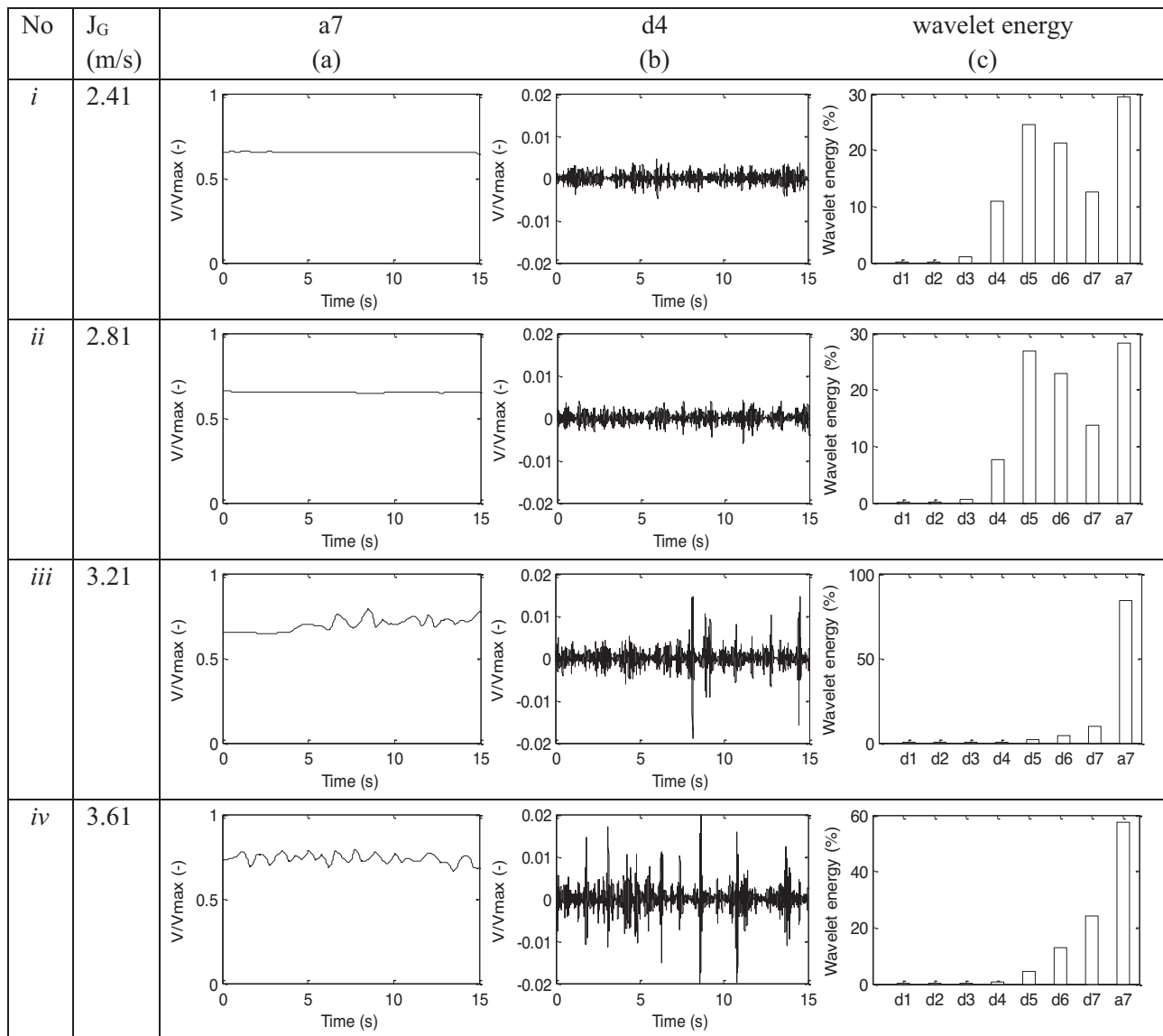


Fig. 12. Typical wavelet analysis of the signals under $J_L = 0.028$ m/s and various gas discharges at $x/L_h = 0.33$.

flow entropy along with the increase in gas flow rate at the low gas supply and a slight increase at high gas supply which corresponds to the random characteristics which are caused by the dynamic of the interface was previously reported by [Catrawedarma et al. \(2021a\)](#), [Catrawedarma et al. \(2021b\)](#). In addition, the increase of entropy which corresponds to the gas flow is in an agreement with [Jin et al. \(2003\)](#) and [Zhang et al. \(2010\)](#) which also obtain that the total flow rate corresponds to the changes of transitional flow pattern. Moreover, [Zhang et al. \(2010\)](#) proposed that the bigger the bubble movement, the higher the loss rate of information, while the self-organization phenomenon causes the decrease in the information loss rate. On the other hand, on a specified gas flow rate, it is noticed that the flow entropy tends to decrease along with the increase of liquid flow rate as shown in [Fig. 11\(b\)](#). The possible reason for this phenomenon is that the random characteristics also correspond to the increase of the liquid flow as well as the gas flow.

3.4. Wavelet analysis

A discrete wavelet transform (DWT) corresponds to the time-frequency analysis in order to reveal the signal characteristics

([Elperin & Klochko, 2002](#); [Zhang et al., 2010](#)). It allows the signal decomposition into several groups of scaled frequencies to obtain the local signal energy distribution during the frequency octaves ([Elperin & Klochko, 2002](#)) which could then be utilized to characterize the fluctuation as the results of air bubble occurrence and movement of the wave ([Catrawedarma et al., 2021a](#)). Furthermore, DWT has been proven as an advanced diagnostic tool in nonlinear multiphase systems specifically to observe the occurrence of frequent breakup and coalescence bubbles, and also continuous movement of interface waves ([Jana et al., 2006](#)). The wavelet spectrum can characterize the flow regimes, while the variances correspond to vector characterization ([Elperin & Klochko, 2002](#)) which enables a flow regime identification through flow behavior assessment ([De Kerpel et al., 2015](#)). Therefore, the clustering by means of artificial neural network on the basis of the wavelet analysis shows a better result than the stochastic analysis ([Catrawedarma et al., 2021b](#)). In addition, the details of wavelet analysis on flow regime identification in a two-phase flow were described by [Elperin & Klochko \(2002\)](#), and also [Morshed et al. \(2020\)](#).

In the present work, a family of wavelet transforms, namely Daubechies 4 (db4), was employed to decompose the parallel-wire probe signals into seven levels with different frequency bands

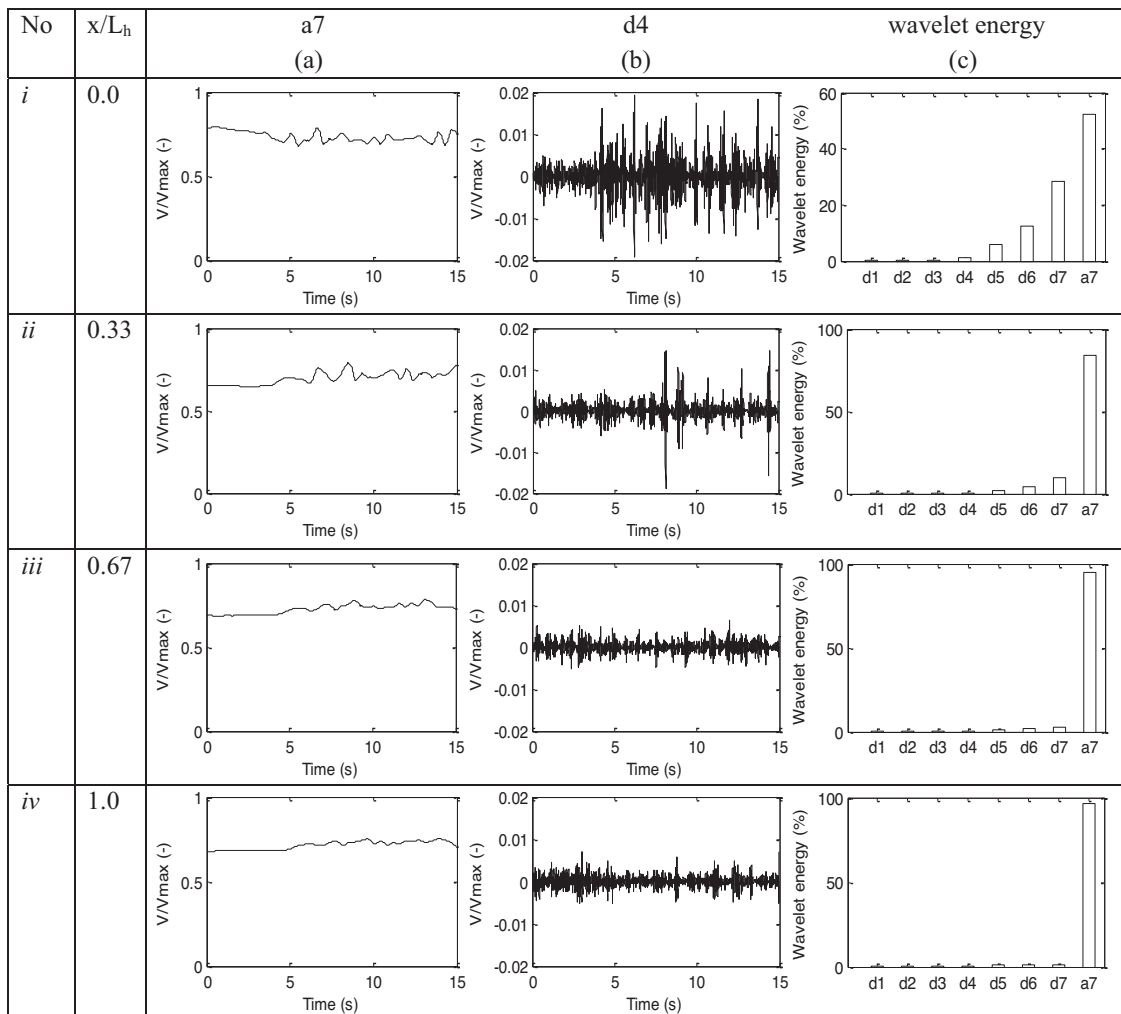


Fig. 13. Typical approximation, detail and wavelet energy under $J_L = 0.028$ m/s and $J_G = 0.48$ m/s at various probe locations.

as previously utilized also by Jana et al. (2006), Zhang et al. (2010), De Kerpel et al. (2015), Morshed et al. (2020), and also Catrawedarma et al. (2021a), Catrawedarma et al. (2021b). Here, $d1$ represents the smallest-scale approximation with a high frequency, while $a7$ corresponds to a largest-scale approximation with a low frequency signal decomposition. Therefore, as the sampling rate on the data acquisition is 1 kHz, the maximum frequency applied to reconstruct entirely signals (Nyquist frequency) is then 500 Hz. Hence, the first decomposed signal or detail $d1$ represents 250–500 Hz, and others frequency bands of sub-signal $d2$, $d3$, $d4$, $d5$, $d6$, $d7$ and $a7$ are 125–250 Hz, 62.5–125 Hz, 31.25–62.5 Hz, 15.625–62.5 Hz, 7.8125–15.625 Hz, 3.90625–7.8125 Hz, and 1.95 3125–3.90625 Hz, respectively. The details of wavelet transform on flow regime identification in a two-phase flow was described by Elperin and Klochko (2002).

The variance distribution representing the wavelet energy of the decomposing signals based on the probe locations under the flow condition of $J_L = 0.028$ m/s and various gas flow rate is described in Fig. 12. It is clearly shown from the figure that the wavelet energy tends to distribute from the detail $d4$ to approximation $a7$. However, in agreement with its PSDF in Fig. 6, it can be notified that the low dominant frequency represents a slug flow during the acquisition. In addition, the frequency fluctuation from $d4$ to $a7$ tends to increase with the increase of gas flow. However, this increase is not directly followed by the increase in wavelet

energy. As shown in column (c), the energy fluctuation of wavelet energy tends to fluctuate along with the increase of the gas flow.

The flow conditions when $J_G = 2.41$ and 2.81 m/s results a similar shape on the detail and approximation. Here, the wavelet analysis as shown in Fig. 12(i) and (ii) indicates that there is no regime change during this parameter change. On the other hand, a sudden rise in the fluctuations in $a7$ and $d5$, as well as an abrupt change of skewness sign and position of its peak in the PDF curve of Fig. 6(ii) and (iii), is orderly shown in Fig. 12(ii) and (iii). The possible reason of this phenomenon can be explained that the drastically fluctuations correspond to a sudden change in a flow regime from separated to intermittent flow as previously reported by Jana et al. (2006). Hence, the particular large fluctuations at $d4$ while $a7$ remains relatively smooth under the condition of $J_G = 2.81$ and 3.21 m/s might correspond to the passage of liquid entrained by gas as also investigated by Jana et al. (2006). Moreover, the wavy interface fluctuations are clearly noticed in Fig. 12(iii) and (iv) on column (a). Another further close observation reveals that when $J_G = 3.21$ m/s, the slug starts to form and is dominant at $J_G = 3.61$ m/s. This trend is also in an agreement with Catrawedarma et al. (2021). Furthermore, during the increase of the gas flow rate, the interface wave fluctuation increases as shown in Fig. 13(a). However, it can be further noticed that the higher the gas flow, the larger the frequency fluctuations as depicted in column (b).

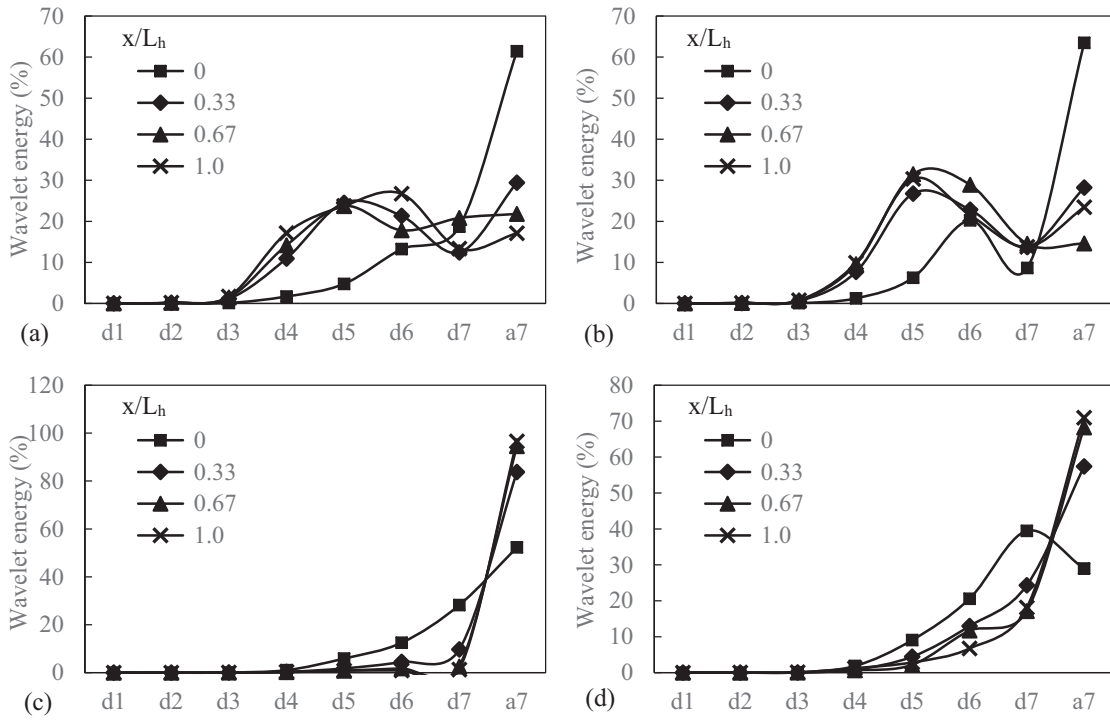


Fig. 14. Wavelet energy under $J_L = 0.028$ m/s, and $J_C =$ (a) 2.41 m/s; (b) 2.81 m/s; (c) 3.21 m/s; (d) 3.61 m/s at various probe locations.

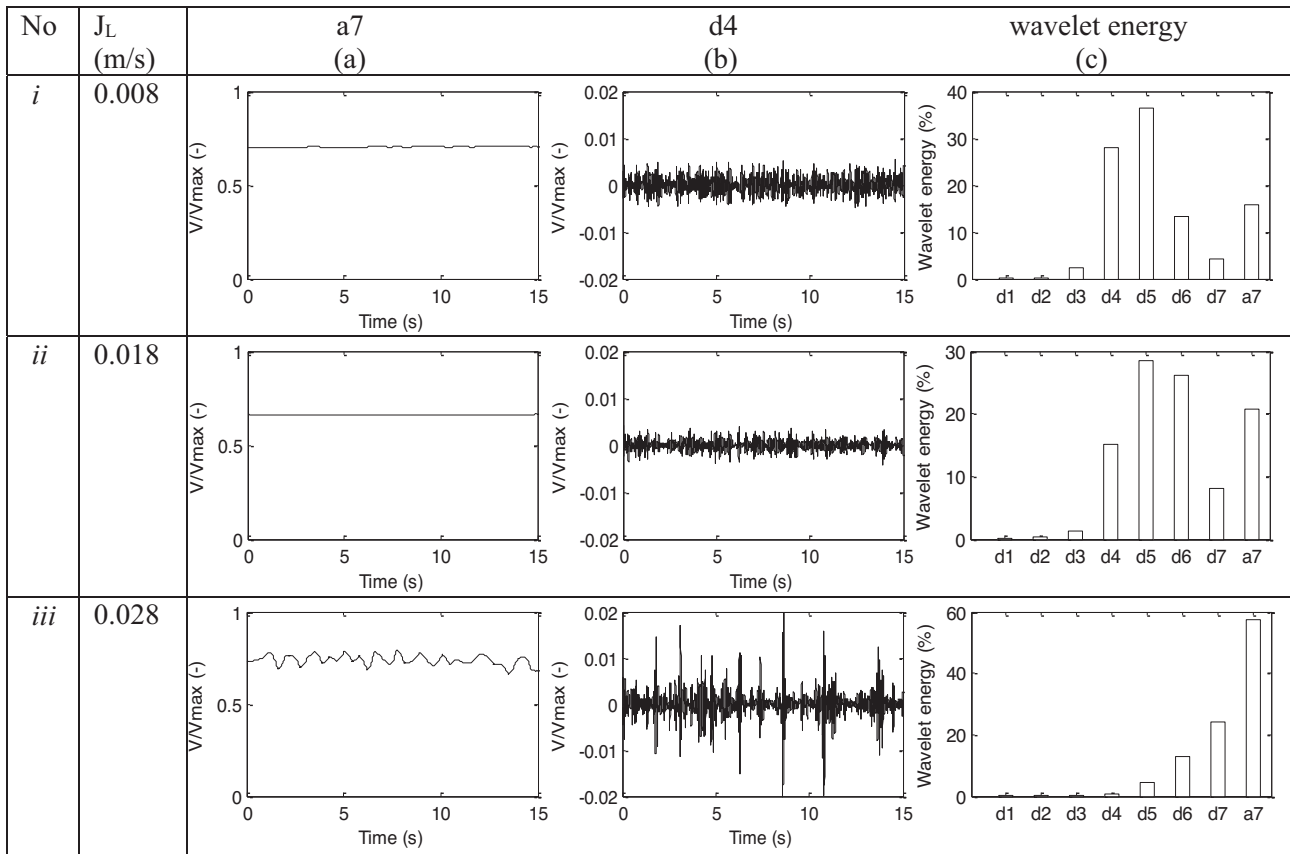


Fig. 15. Typical wavelet analysis of the signals under $J_C = 3.61$ m/s and various liquid discharges at $x/L_h = 0.33$.

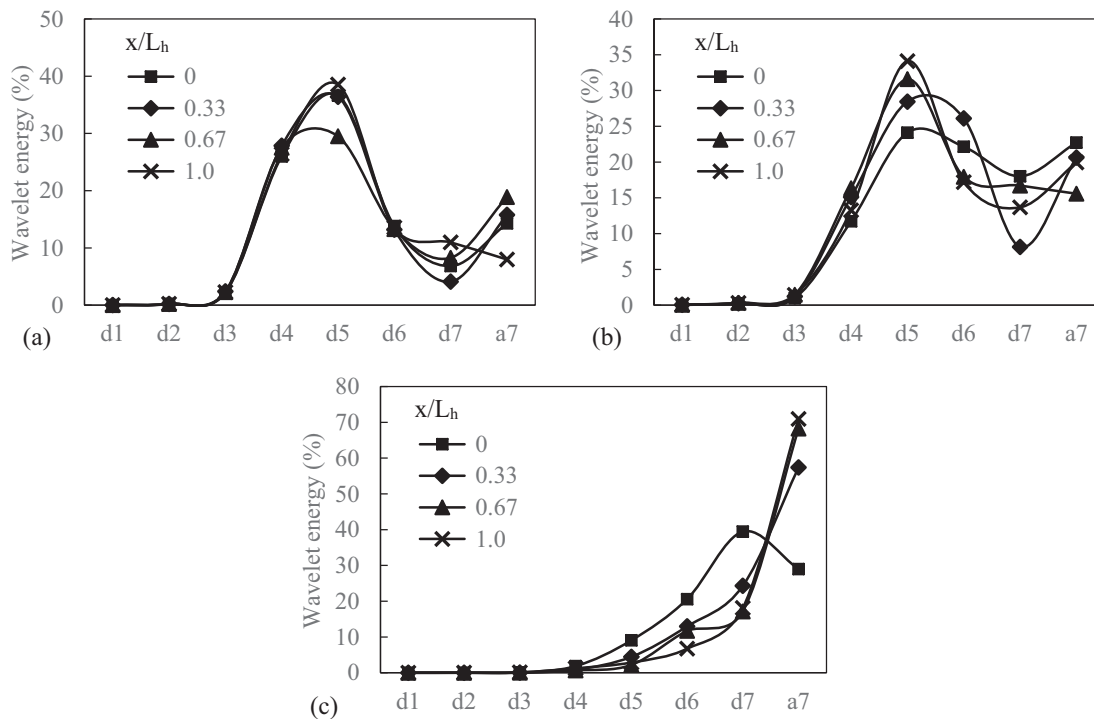


Fig. 16. The wavelet energy under $J_G = 3.61$ m/s, and (a) $J_L = 0.008$ m/s; (b) $J_L = 0.018$ m/s; (c) $J_L = 0.028$ m/s at various probe locations.

Moreover, the interface wave fluctuations tend to decrease along with the sensor location shifts closer to the liquid exit as depicted in Fig. 13 column (a). However, the nearer the location to the bend, the larger the obtained energy fluctuations of the dynamic process as shown in column (b). Therefore, the closer the locus to the liquid exit, the higher the obtained wavelet energy at the approximation as depicted in column (c). A closer observation through video recording towards this phenomenon reveals that the nearer the location to the liquid exit, the lower the frequency of either liquid blockage or slug.

Fig. 14 shows the comparison of the wavelet energy on various of the locus and gas flow rates under a constant of $J_L = 0.028$ m/s. From the figure, it is noticed that all locus correlates a certain trend by the increase in gas flow. At the low gas flow rates ($J_G = 2.41$ and 2.81 m/s), where the obtained flow pattern was stratified regimes, such relatively similar trends in all locus are obtained. Here, the wavelet energy are distributed from $d4$ and reach on their peaks at $d5$, whereas at the $x/L_h = 0$ consistently shows the highest energy on its approximation. Furthermore, at the higher gas flow rates ($J_G = 3.21$ and 3.61 m/s), where the onset of liquid blockage and the intermittent regimes were obtained, another relatively similar trends of all locus are also obtained. Here, the wavelet energy are distributed from $d5$, and reaches their peaks at $a7$.

In addition, the comparison of the wavelet energy as a function of the liquid flow is shown in Fig. 15. From the figure, it can be seen that the wavelet energies are distributed from $d4$ to $a7$. Moreover, at the highest liquid flow rate ($J_L = 0.028$ m/s), the wavelet energy is distributed and dominantly reaches its peak at $a7$ which corresponds to a large-scale approximation with a low frequency. In agreement with the PSDF as shown in Fig. 9, it is noticed that the low dominant frequency represents the occurrence of slug in the test section. Here, as the fluctuations of the wavy interface are clearly depicted in Fig. 15(iii), a close observation of the video recording also reveals the formed slug is dominant. Additionally, the wave interface and frequency fluctuations tend to increase with the increase of gas flow as depicted in Fig. 15 column (a) and (b).

Fig. 16 shows another wavelet energy comparison on various of the locus and the liquid flow rates under a constant of $J_G = 3.61$ m/s. From the figure, it is noticed that all locus correlates a clear trend by the increase in liquid flow rate. At lower liquid flow rates ($J_L = 0.008$ and 0.018 m/s) under the flow condition was stratified, such relatively similar trends in all locus are also obtained. Here, the wavelet energy are distributed from $d4$ and reach on their peaks at $d5$. Furthermore, at a higher liquid flow rate ($J_L = 0.028$ m/s) where the detected flow pattern was an intermittent, another relatively similar trend of all locus are also obtained. Here, the wavelet energy are distributed from $d5$, and reach their peaks at $a7$.

4. Concluding remarks

An attempt to characterize the interfacial behaviors through the liquid film fluctuations' data during gas-liquid counter-current flow on a complex geometry representing 1/30 scaled-down PWR hot leg has been carried out. Such advanced statistical tools namely PDF, PSDF, Kolmogorov entropy, and wavelet transform were employed to elaborate the flow characteristics. Several remarks are summarized as follows:

- The flow development during the flooding mechanism involves the liquid film thickening combined by an unstable of the interface which is caused by the increase of the gas discharge. This triggers the liquid blockage to initiate the CCFL and followed by the occurrence of slug and churn flows.
- As the increase of the liquid flow, the signal fluctuations tend to decrease along with the location shifts closer to the liquid exit. On the other hand, it results on the decrease of liquid film thickness. Moreover, the onset of liquid blockage is indicated by multimodal PDF, whereas the stratified regime approaches unimodal PDF which corresponds to the number of dominant film thickness.

- c. Stratified flow is characterized by a unimodal PDF, while its frequency and wavy interface fluctuations tend to be smooth. Here, the wavelet energy distributes from d_5 to d_7 . On the other hand, the slug flow is characterized by fluctuations in the frequency and wavy interface forms a multimodal PDF. Here, the energy fluctuation increases gradually from d_1 to d_7 .

Declaration of Competing Interest

The authors declare that they have no known competing financial interests or personal relationships that could have appeared to influence the work reported in this paper.

Acknowledgments

The authors would like to acknowledge the Direktorat Pendidikan Tinggi (DIKTI) and Direktorat Riset dan Pengabdian Masyarakat (DRPM) Kementerian Pendidikan, Kebudayaan, Riset dan Teknologi (KEMENDIKBUD-RISTEK) Republic of Indonesia for the research funding of BPPDN 2019 and PDD 2021 (contract number: 2303/UN1/DITLIT/DIT-LIT/PT/2021), respectively. We are also grateful to Dr. Apip Badarudin, Setya Wijayanta, Akhlisa Nadiantya Aji Nugroho, Mucshin Muzafar Rasyidi, Yulia Venti Yoanita and also Christina Deni Rumiarti for their technical supports during the manufacturing of the apparatus or the data tabulation assistances. During a better understanding toward the interfacial behavior, visualizations were also largely captured by using a Phantom Miro Lab310 high speed video camera. Therefore, we also acknowledge Chevron Indonesia for the opportunity.

References

- Al Issa, S., Macian-Juan, R., 2011. A review of CCFL phenomenon. *Ann. Nucl. Energy* 38 (9), 1795–1819. <https://doi.org/10.1016/j.anucene.2011.04.021>.
- Al Issa, S., Macian-Juan, R., 2014. Experimental investigation of countercurrent flow limitation (CCFL) in a large-diameter hot-leg geometry: a detailed description of CCFL mechanisms, flow patterns and high-quality HSC imaging of the interfacial structure in a 1/3.9 scale of PWR geometry. *Nucl. Eng. Des.* 280, 550–563. <https://doi.org/10.1016/j.nucengdes.2014.08.021>.
- Al Issa, S., Macian-Juan, R., 2017. Image-processing of time-averaged interface distributions representing CCFL characteristics in a large scale model of a PWR hot-leg pipe geometry. *Ann. Nucl. Energy* 103, 282–293. <https://doi.org/10.1016/j.anucene.2017.01.021>.
- Astyanto, A.H., Rahman, Y., Adhikara, A.Y., Indarto, & Deendarlianto, 2021a. Time-series differential pressure fluctuations of a flooding regime : A preliminary experimental results investigation on a 1 / 30 down- scaled PWR hot leg geometry. *AIP Conf. Proc.* 060001 (2011).
- Astyanto, A.H., Rahman, Y., Medha, A.Y.A., Deendarlianto, D., Indarto, I., 2021b. Pengaruh Rasio I/D terhadap Permulaan Flooding dan Fluktuasi Voltase Sinyal Tekanan Rezim Flooding pada Geometri Kompleks. *Rekayasa Mesin* 12 (2), 447–457.
- Badarudin, A., Indarto, D., Setyawan, A., 2016. Characteristics of the air-water counter current two-phase flow in a 1/30 scale of pressurized water reactor (PWR): Interfacial behavior and CCFL data. *AIP Conf. Proc.* 1737. <https://doi.org/10.1063/1.4949303>.
- Badarudin, A., Pinindriya, S. T., Yoanita, Y. V., Hadipranoto, M. S., Hartono, S., Ariawan, R., Indarto, Deendarlianto., 2018. The effect of horizontal pipe length to the onset of flooding position on the air-water counter current two-phase flow in a 1/30 scale of pressurized water reactor (PWR). *AIP Conference Proceedings*, 2001 (June 2020). <https://doi.org/10.1063/1.5049983>.
- Badarudin, A., Setyawan, A., Dinaryanto, O., Widyatama, A., Indarto, & Deendarlianto, 2018b. Interfacial behavior of the air-water counter-current two-phase flow in a 1/30 scale-down of pressurized water reactor (PWR) hot leg. *Ann. Nucl. Energy* 116, 376–387. <https://doi.org/10.1016/j.anucene.2018.03.007>.
- Canière, H., T'Joen, C., Willockx, A., Paepé, M.D., Christians, M., Rooyen, E.van., Liebenberg, L., Meyer, J.P., 2007. Horizontal two-phase flow characterization for small diameter tubes with a capacitance sensor. *Meas. Sci. Technol.* 18 (9), 2898–2906. <https://doi.org/10.1088/0957-0233/18/9/020>.
- Catrawedarma, I.G.N.B., Deendarlianto, Indarto, 2021a. Statistical characterization of flow structure of air–water two-phase flow in airlift pump–bubble generator system. *Int. J. Multiph. Flow* 138, 103596. <https://doi.org/10.1016/j.ijmultiphaseflow.2021.103596>.
- Catrawedarma, I.G.N.B., Resnaraditya, F.A., Deendarlianto, Indarto, 2021b. Statistical characterization of the flow Structure of air–water–solid particles three-phase flow in the airlift pump–bubble generator system. *Flow Meas. Instrum.* 82, 102062. <https://doi.org/10.1016/j.flowmeasinst.2021.102062>.
- Choi, K.Y., No, H.C., 1995. Experimental studies of flooding in nearly horizontal pipes. *Int. J. Multiph. Flow* 21 (3), 419–436. [https://doi.org/10.1016/0301-9322\(94\)00087-2](https://doi.org/10.1016/0301-9322(94)00087-2).
- De Kerpel, K., De Schampheleire, S., De Keulenaer, T., De Paepé, M., 2015. Two-phase flow regime assignment based on wavelet features of a capacitance signal. *Int. J. Heat Fluid Flow* 56, 317–323. <https://doi.org/10.1016/j.ijheatfluidflow.2015.09.002>.
- Deendarlianto, D., Höhne, T., Lucas, D., Vallée, C., Zabala, G.A.M., 2011. CFD studies on the phenomena around counter-current flow limitations of gas/liquid two-phase flow in a model of a PWR hot leg. *Nucl. Eng. Des.* 241 (12), 5138–5148. <https://doi.org/10.1016/j.nucengdes.2011.08.071>.
- Deendarlianto, Höhne, T., Lucas, D., Vierow, K., 2012. Gas-liquid countercurrent two-phase flow in a PWR hot leg: a comprehensive research review. *Nucl. Eng. Des.* 243, 214–233. <https://doi.org/10.1016/j.nucengdes.2011.11.015>.
- Deendarlianto, Ousaka, A., Indarto, Kariyasaki, A., Lucas, D., Vierow, K., Vallee, C., Hogan, K., 2010. The effects of surface tension on flooding in counter-current two-phase flow in an inclined tube. *Exp. Therm Fluid Sci.* 34 (7), 813–826. <https://doi.org/10.1016/j.expthermflusci.2010.01.010>.
- Deendarlianto, Ousaka, A., Kariyasaki, A., Fukano, T., 2005. Investigation of liquid film behavior at the onset of flooding during adiabatic counter-current air-water two-phase flow in an inclined pipe. *Nucl. Eng. Des.* 235 (21), 2281–2294. <https://doi.org/10.1016/j.nucengdes.2005.03.006>.
- Deendarlianto, Vallée, C., Lucas, D., Beyer, M., Pietruske, H., Carl, H., 2008. Experimental study on the air/water counter-current flow limitation in a model of the hot leg of a pressurized water reactor. *Nucl. Eng. Des.* 238 (12), 3389–3402. <https://doi.org/10.1016/j.nucengdes.2008.08.003>.
- Dos Reis, E., Goldstein, L.J., 2010. Characterization of slug flows in horizontal piping by signal analysis from a capacitive probe. *Flow Meas. Instrum.* 21 (3), 347–355. <https://doi.org/10.1016/j.flowmeasinst.2010.04.006>.
- Elperin, T., Klochko, M., 2002. Flow regime identification in a two-phase flow using wavelet transform. *Exp. Fluids* 32 (6), 674–682. <https://doi.org/10.1007/s00348-002-0415-x>.
- Ghiaasiaan, S.M., Wu, X., Sadowski, D.L., Abdel-Khalik, S.I., 1997. Hydrodynamic characteristics of counter-current two-phase flow in vertical and inclined channels: Effects of liquid properties. *Int. J. Multiph. Flow* 23 (6), 1063–1083. [https://doi.org/10.1016/s0301-9322\(97\)00027-x](https://doi.org/10.1016/s0301-9322(97)00027-x).
- Ghosh, S., Pratihari, D.K., Maiti, B., Das, P.K., 2012. Identification of flow regimes using conductivity probe signals and neural networks for counter-current gas-liquid two-phase flow. *Chem. Eng. Sci.* 84, 417–436. <https://doi.org/10.1016/j.ces.2012.08.042>.
- Ghosh, S., Pratihari, D.K., Maiti, B., Das, P.K., 2013. Automatic classification of vertical counter-current two-phase flow by capturing hydrodynamic characteristics through objective descriptions. *Int. J. Multiph. Flow* 52, 102–120. <https://doi.org/10.1016/j.ijmultiphaseflow.2012.12.007>.
- Glaeser, H., Karwat, H., 1993. The contribution of UPTF experiments to resolve some scale-up uncertainties in countercurrent two phase flow. *Nucl. Eng. Des.* 145 (1–2), 63–84. [https://doi.org/10.1016/0029-5493\(93\)90059-1](https://doi.org/10.1016/0029-5493(93)90059-1).
- Grassberger, P., Procaccia, I., 1983. Estimation of the Kolmogorov entropy for a chaotic signal. *Phys. Rev.* 28 (4), 2591–2593.
- Hudaya, A.Z., Widyatama, A., Dinaryanto, O., Juwana, W.E., Indarto, & Deendarlianto, 2019. The liquid wave characteristics during the transportation of air-water stratified co-current two-phase flow in a horizontal pipe. *Exp. Therm Fluid Sci.* 103 (January), 304–317. <https://doi.org/10.1016/j.expthermflusci.2019.01.021>.
- Jana, A.K., Das, G., Das, P.K., 2006. Flow regime identification of two-phase liquid-liquid upflow through vertical pipe. *Chem. Eng. Sci.* 61 (5), 1500–1515. <https://doi.org/10.1016/j.ces.2005.09.001>.
- Jin, N.D., Nie, X.B., Ren, Y.Y., Liu, X.B., 2003. Characterization of oil/water two-phase flow patterns based on nonlinear time series analysis. *Flow Meas. Instrum.* 14 (4–5), 169–175. [https://doi.org/10.1016/S0955-5986\(03\)00022-0](https://doi.org/10.1016/S0955-5986(03)00022-0).
- Johnsson, F., Zijerveld, R.C., Schouten, J.C., Van Den Bleek, C.M., Leckner, B., 2000. Characterization of fluidization regimes by time-series analysis of pressure fluctuations. *Int. J. Multiph. Flow* 26 (4), 663–715. [https://doi.org/10.1016/S0301-9322\(99\)00028-2](https://doi.org/10.1016/S0301-9322(99)00028-2).
- Kinoshita, I., Nriai, T., Tomiyama, A., Lucas, D., Murase, M., 2011. Effects of liquid properties on CCFL in a scaled-down model of a PWR hot leg. *J. Power Energy Syst.* 5 (3), 316–329. <https://doi.org/10.1299/jpes.5.316>.
- Koskie, J.E., Mudawar, I., Tiederman, W.G., 1989. Parallel-wire probes for measurement of thick liquid films. *Int. J. Multiph. Flow* 15 (4), 521–530. [https://doi.org/10.1016/0301-9322\(89\)90051-7](https://doi.org/10.1016/0301-9322(89)90051-7).
- Lucas, D., Beyer, M., Pietruske, H., Szalinski, L., 2017. Counter-current flow limitation for air-water and steam-water flows in a PWR hot leg geometry. *Nucl. Eng. Des.* 323 (April), 56–67. <https://doi.org/10.1016/j.nucengdes.2017.07.032>.
- Mayinger, F., Weiss, P., Wolfert, K., 1993. Two-phase flow phenomena in full-scale reactor geometry. *Nucl. Eng. Des.* 145 (1–2), 47–61. [https://doi.org/10.1016/0029-5493\(93\)90058-H](https://doi.org/10.1016/0029-5493(93)90058-H).
- Minami, N., Nishiwaki, D., Nariai, T., Tomiyama, A., Murase, M., 2010. Countercurrent gas-liquid flow in a pwr hot leg under reflux cooling (i) air-water tests for 1/15-scale model of a pwr hot leg. *J. Nucl. Sci. Technol.* 47 (2), 142–148. <https://doi.org/10.1080/18811248.2010.9711938>.
- Morshed, M., Khan, M.S., Rahman, M.A., Imtiaz, S., 2020. Flow regime, slug frequency and wavelet analysis of air/Newtonian and air/non-Newtonian

- two-phase flow. *Applied Sciences* (Switzerland) 10 (9), 3272. <https://doi.org/10.3390/app10093272>.
- Navarro, M.A., 2005. Study of countercurrent flow limitation in a horizontal pipe connected to an inclined one. *Nucl. Eng. Des.* 235 (10–12), 1139–1148. <https://doi.org/10.1016/j.nucengdes.2005.02.010>.
- Nguyen, V.T., Euh, D.J., Song, C.H., 2010. An application of the wavelet analysis technique for the objective discrimination of two-phase flow patterns. *Int. J. Multiph. Flow* 36 (9), 755–768. <https://doi.org/10.1016/j.ijmultiphaseflow.2010.04.007>.
- Ohnuki, A., 1986. Experimental study of counter-current two-phase flow in horizontal tube connected to inclined riser. *J. Nucl. Sci. Technol.* 23 (3), 219–232. <https://doi.org/10.1080/18811248.1986.9734975>.
- Ousaka, A., Deendarlianto, Kariyasaki, A., Fukano, T., 2006. Prediction of flooding gas velocity in gas-liquid counter-current two-phase flow in inclined pipes. *Nucl. Eng. Des.* 236 (12), 1282–1292. <https://doi.org/10.1016/j.nucengdes.2005.12.001>.
- Petrtsch, G., Mewes, D., 1999. Experimental investigations of the flow patterns in the hot leg of a pressurized water reactor. *Nucl. Eng. Des.* 188 (1), 75–84. [https://doi.org/10.1016/S0029-5493\(99\)00005-9](https://doi.org/10.1016/S0029-5493(99)00005-9).
- Prayitno, S., Santoso, R.A., Deendarlianto, Höhne, T., Lucas, D., 2012. Counter current flow limitation of gas-liquid two-phase flow in nearly horizontal pipe. *Sci. Technol. Nucl. Install.* 2012, 1–9. <https://doi.org/10.1155/2012/513809>.
- Rodrigues, R.L.P., Cozin, C., Naidiek, B.P., Marcelino Neto, M.A., da Silva, M.J., Morales, R.E.M., 2020. Statistical features of the flow evolution in horizontal liquid-gas slug flow. *Exp. Therm Fluid Sci.* 119, 110203. <https://doi.org/10.1016/j.expthermflusci.2020.110203>.
- Samal, K., Ghosh, S., 2021. Kerosene-water counter-current two-phase flow-structures varying flow-orientation in 15 mm diameter duct. *Flow Meas. Instrum.* 81, (July). <https://doi.org/10.1016/j.flowmeasinst.2021.102016> 102016.
- Setyawan, A., Indarto, & Deendarlianto, 2016. The effect of the fluid properties on the wave velocity and wave frequency of gas-liquid annular two-phase flow in a horizontal pipe. *Exp. Therm Fluid Sci.* 71, 25–41. <https://doi.org/10.1016/j.expthermflusci.2015.10.008>.
- Setyawan, A., Indarto, & Deendarlianto, 2017. Experimental investigations of the circumferential liquid film distribution of air-water annular two-phase flow in a horizontal pipe. *Exp. Therm Fluid Sci.* 85, 95–118. <https://doi.org/10.1016/j.expthermflusci.2017.02.026>.
- Siddiqui, H., Banerjee, S., Ardron, K.H., 1986. Flooding in a N elbow between a vertical a N D a horizontal or near-horizontal pipe. *Int. J. Multiph. Flow* 12 (4), 531–541.
- Vallée, C., Nariai, T., Futatsugi, T., Tomiyama, A., Lucas, D., Murase, M., 2012a. Experimental characterisation of the interfacial structure during counter-current flow limitation in a model of the hot leg of a PWR. *Sci. Technol. Nucl. Install.* 2012, 1–8. <https://doi.org/10.1155/2012/298452>.
- Vallée, C., Seidel, T., Lucas, D., Beyer, M., Prasser, H.M., Pietruske, H., Schütz, P., Carl, H., 2012b. Counter-current flow limitation in a model of the hot leg of a PWR - Comparison between air/water and steam/water experiments. *Nucl. Eng. Des.* 245, 113–124. <https://doi.org/10.1016/j.nucengdes.2012.01.001>.
- Van Ommen, J.R., Sasic, S., Van der Schaaf, J., Gheorghiu, S., Johnsson, F., Coppens, M. O., 2011. Time-series analysis of pressure fluctuations in gas-solid fluidized beds – a review. *Int. J. Multiph. Flow* 37 (5), 403–428. <https://doi.org/10.1016/j.ijmultiphaseflow.2010.12.007>.
- Wijayanta, S., Indarto, Deendarlianto, Catrawedarma, I., & Hudaya, A. Z. in press. Statistical Characterization of the Interfacial Behavior of the Gas-Liquid Stratified Two-Phase Flow in a Horizontal Pipe. *Flow Measure. Instrument.*
- Wongwises, S., 1994. Experimental investigation of two-phase countercurrent flow limitation in a bend between horizontal and inclined pipes. *Exp. Therm. Fluid Sci.* 8 (3), 245–259.
- Zapke, A., Kröger, D.G., 1996. The influence of fluid properties and inlet geometry on flooding in vertical and inclined tubes. *Int. J. Multiphase Flow* 22 (3), 461–472. [https://doi.org/10.1016/0301-9322\(95\)00076-3](https://doi.org/10.1016/0301-9322(95)00076-3).
- Zhang, W.H., Li, H., Li, X., 2010. Identification of regime transitions in an inner-loop airlift reactor using local bubble-induced pressure fluctuation signals. *Chem. Eng. J.* 162 (1), 296–300. <https://doi.org/10.1016/j.cej.2010.04.038>.
- Zhou, Y., Jin, N., Zhang, H., Zhai, L., 2020. Method based on parallel-wire conductivity probe for measuring water hold-up in near-horizontal oil–water two-phase flow pipes. *IET Sci., Measur. Technol.* 14 (6), 676–683. <https://doi.org/10.1049/iet-smt.2019.0308>.